J|A|C|S

A R T I C L E S

Ultralarge Hyperpolarizability Twisted π-Electron System Electro-Optic Chromophores: Synthesis, Solid-State and Solution-Phase Structural Characteristics, Electronic Structures, Linear and Nonlinear Optical Properties, and Computational Studies

Hu Kang,[†] Antonio Facchetti,[†] Hua Jiang,[†] Elena Cariati,[‡] Stefania Righetto,[‡]
Renato Ugo,[‡] Cristiano Zuccaccia,[§] Alceo Macchioni,[§] Charlotte L. Stern,[†] Zhifu Liu,[ǁ]
Seng-Tiong Ho,[ǁ] Eric C. Brown,[†] Mark A. Ratner,[†] and Tobin J. Marks*,[†]

*Contribution from the Department of Chemistry and the Materials Research Center and
Department of Electrical and Computer Engineering, Northwestern University, 2145 Sheridan
Road, Evanston, Illinois 60208-3113, Dipartimento di Chimica Inorganica Metallorganica e
Analitica e Centro di Eccellenza CIMAINA dell'Università di Milano and Unità di Ricerca
dell'INSTM di Milano, Via Venezian 21, I-20133 Milano, Italy, and Dipartimento di Chimica,
Università di Perugia,Via Elce di Sotto 8, I-06123 Perugia, Italy*

Received October 24, 2006; E-mail: t-marks@northwestern.edu

Abstract: This contribution details the synthesis and chemical/physical characterization of a series of unconventional twisted π-electron system electro-optic (EO) chromophores. Crystallographic analysis of these chromophores reveals large ring−ring dihedral twist angles (80−89°) and a highly charge-separated zwitterionic structure dominating the ground state. NOE NMR measurements of the twist angle in solution confirm that the solid-state twisting persists essentially unchanged in solution. Optical, IR, and NMR spectroscopic studies in both the solution phase and solid state further substantiate that the solid-state structural characteristics persist in solution. The aggregation of these highly polar zwitterions is investigated using several experimental techniques, including concentration-dependent optical and fluorescence spectroscopy and pulsed field gradient spin−echo (PGSE) NMR spectroscopy in combination with solid-state data. These studies reveal clear evidence of the formation of centrosymmetric aggregates in concentrated solutions and in the solid state and provide quantitative information on the extent of aggregation. Solution-phase DC electric-field-induced second-harmonic generation (EFISH) measurements reveal unprecedented hyperpolarizabilities (nonresonant $\mu\beta$ as high as $-488\,000 \times 10^{-48}$ esu at 1907 nm). Incorporation of these chromophores into guest−host poled polyvinylphenol films provides very large electro-optic coefficients (r_{33}) of ∼330 pm/V at 1310 nm. The aggregation and structure−property effects on the observed linear/nonlinear optical properties are discussed. High-level computations based on state-averaged complete active space self-consistent field (SA-CASSCF) methods provide a new rationale for these exceptional hyperpolarizabilities and demonstrate significant solvation effects on hyperpolarizabilities, in good agreement with experiment. As such, this work suggests new paradigms for molecular hyperpolarizabilities and electro-optics.

Introduction

The development of high-performance molecule-based electro-optic (EO) materials has been the focus of much current research. Such materials are of great scientific and technological interest not only for applications as diverse as optical telecommunications, signal processing, data storage, image reconstruction, logic technologies, and optical computing, but also for the fundamental understanding of how matter interacts with light.[1−3]

The essential requirement for large bulk EO response is that the active component chromophores have a large microscopic molecular first hyperpolarizability tensor (β), and the quest for such chromophores has been a very active research field.[1−3] To date, the vast majority of effective EO chromophores have been devised according to very similar design principles: planar

† Department of Chemistry and the Materials Research Center, Northwestern University.
‡ Università di Milano.
§ Università di Perugia.
ǁ Department of Electrical and Computer Engineering, Northwestern University.

(1) (a) Dalton, L. R. *Pure Appl.Chem.* **2004**, *76,* 1421. (b) Kajzar, F.; Lee, K.-S. A.; Jen, K.-Y. *Adv. Polym. Sci.* **2003**, *161*, 1. (c) Dalton, L. R. *Adv. Polym. Sci.* **2002**, *158*, 1. (d) Dalton, L. R.; Steier, W. H.; Robinson, B. H.; Zhang, C.; Ren, A.; Garner, S.; Chen, A.; Londergan, T.; Irwin, L.; Carlson, B.; Fifield, L.; Phelan, G.; Kincaid, C.; Amend, J.; Jen, A. *J. Mater. Chem.* **1999**, *9*, 1905. (e) Molecular Nonlinear Optics: Materials, Phenomena and Devices (Zyss, J., Ed.). *Chem. Phys.* **1999**, *245* (Special issue). (f) Verbiest, T.; Houbrechts, S.; Kauranen, M.; Clays, K.; Persoons, A. *J. Mater. Chem.* **1997**, *7*, 2175. (g) Marks, T. J.; Ratner, M. A. *Angew. Chem., Int. Ed. Engl.* **1995**, *34*, 155.

conjugated π-electron systems end capped with electron-donor and -acceptor (D, A) moieties. This design algorithm gives rise to a dominant intramolecular charge-transfer (ICT) transition from the ground state to the first excited state and produces effective polarization along the π-conjugated axis. Considerable efforts[4] have been directed toward the molecular engineering of such chromophore structures, and a variety of strategies has emerged within the framework of the classical "two-state model" for molecular hyperpolarizability β.[5] This simple model invokes a polar ground state and a charge-separated first excited state, where β is determined by the energy gap between the two states (ΔE_{ge}), the transition dipole moment (μ_{ge}) between the two states, and the difference in dipole moment between the two states ($\Delta\mu_{ge} = \mu_{ee} - \mu_{gg}$) (eq 1).

$$\beta \propto \Delta\mu_{ge}(\mu_{ge})^2/(\Delta E_{ge})^2 \tag{1}$$

One approach to enhancing β proposed by Marder and co-workers involves tuning "bond length alternation" (BLA; the difference between average single and double bond lengths in the conjugated chromophore core).[6] They argued that BLA, hence β, can be optimized by controlling the relative neutral and charge-separated contributions to the ground state via modifying D/A substituent strength, the polarity of the solvent, or the strength of an applied electric field. Another model, "auxiliary donors and acceptors",[7] correlates molecular hyper-polarizability with the electron density of the π conjugation, arguing that electron-excessive/deficient heterocycle bridges act as auxiliary donors/acceptors and lead to substantial increases in β values. Directed by these strategies, the largest hyperpolarizabilities have, to date, been observed with protected polyene

and/or multiple (including fused) thiophene ring-containing bridges (e.g., **CLD** and **FTC**), with the chromophore figures-of-merit, $\mu\beta$ (μ = the molecular dipole moment), as high as $35\,000 \times 10^{-48}$ esu being achieved.[3d]
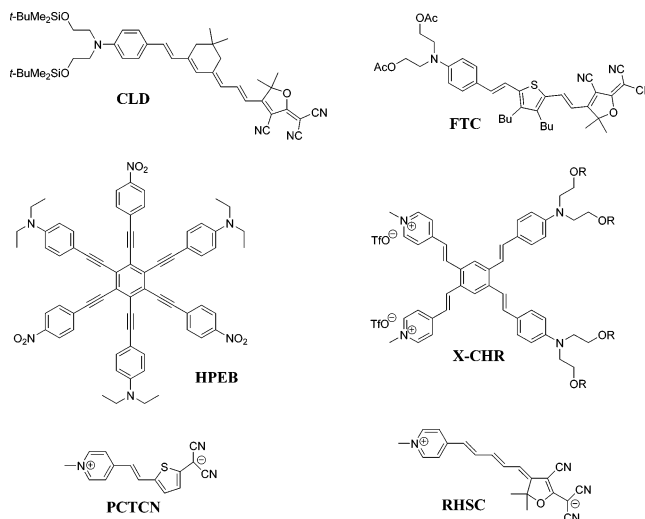
Note that such strategies focus primarily on extensive *planar* π conjugation and that such molecules are inherently structurally complex, complicating synthetic access and introducing potential chemical, thermal, and photochemical frailties.[8] Furthermore, extended conjugated systems typically introduce bathochromic shifts in optical excitation, thus eroding transparency at the near-IR working wavelengths of many photonic applications. Other β enhancement strategies have emerged recently, including multidimensional charge-transfer chromophores (e.g., **HPEB** and **X**-**CHR**)[9] and a class of "right-hand-side" zwitterionic chromophores (e.g., **PCTCN** and **RHSC**).[4d,10] These chromophores exhibit improved transparency and stability but not significant enhancement in hyperpolarizability. Interestingly, Kuzyk has argued that the β responses of all known organic EO chromophores fall far short of the fundamental quantum limits by a factor of $\sim10^{-3/2}$ for reasons that are presently not entirely clear but the understanding of which may afford

(2) (a) *Characterization Techniques and Tabulations for organic Nonlinear Optical Materials*; Kuzyk, M. G., Dirk, C. W., Eds.; Marcel Dekker: New York, 1998. (b) *Nonlinear Optics of Organic Molecules and Polymers*; Nalwa, H. S., Miyata, S., Eds.; CRC Press: Boca Raton, FL, 1997. (c) *Organic Nonlinear Optical Materials*; Bosshard, Ch., Sutter, K., Prêtre, Ph., Hulliger, J., Flörsheimer, M., Kaatz, P., Günter, P., Eds.; Advances in Nonlinear Optics; Gordon & Breach Amsterdam, 1995; Vol. 1. (d) *Molecular Nonlinear Optics: Materials, Physics, Devices*; Zyss, J., Ed.; Academic Press: Boston, MA, 1994. (e) *Introduction to Nonlinear Optical Effects in Molecules and Polymers*; Prasad, P. N., Williams, D. J., Eds.; John Wiley: New York, 1991. (f) *Materials for Nonlinear Optics Chemical Perspectives*; Marder, S. R., Stucky, G. D., Sohn, J. E., Eds.; ACS Symposium Series 455; American Chemical Society: Washington, DC, 1991.

(3) (a) Dalton, L. R.; Jen, A. K.-Y.; Steier, W. H.; Robinson, B. H.; Jang, S.-H.; Clot, O.; Song, H. C.; Kuo, Y.-H.; Zhang, C.; Rabiei, P.; Ahn, S.-W.; Oh, M. C. *SPIE Proc.* **2004**, *5351*, 1. (b) Lee, M.; Katz, H. E.; Erben, C.; Gill, D. M.; Gopalan, P.; Heber, J. D.; McGee, D. J. *Science* **2002**, *298*, 1401. (c) Ma, H.; Jen, A. K. Y.; Dalton, L. R. *Adv. Mater.* **2002**, *14*, 1339. (d) Shi, Y.; Zhang, C.; Zhang, H.; Bechtel, J. H.; Dalton, L. R.; Robinson, B. H.; Steier, W. H. *Science* **2000**, *28*, 119.

(4) (a) Liao, Y.; Eichinger, B. E.; Firestone, K. A.; Haller, M.; Luo, J.; Kaminsky, W.; Benedict, J. B.; Reid, P. J.; Jen, A. K.-Y.; Dalton, L. R.; Robinson, B. H. *J. Am. Chem. Soc.* **2005**, *127*, 2758. (b) Andreu, R.; Blesa, M. J.; Carrasquer, L.; Garín, J.; Orduna, J.; Villacampa, B.; Alcalá, R.; Casado, J.; Delgado, M. C. R.; Navarrete, J. T. L.; Allain, M. *J. Am. Chem. Soc.* **2005**, *127*, 8835. (c) Staub, K.; Levina, G. A.; Barlow, S.; Kowalczyk, T. C.; Lackritz, H. S.; Barzoukas, M.; Fort, A.; Marder, S. R. *J. Mater. Chem.* **2003**, *13*, 825. (d) Abbotto, A.; Beverina, L.; Bradamante, S.; Facchetti, A.; Klein, C.; Pagani, G. A.; Redi-Abshiro, M.; Wortmann, R. *Chem. Eur. J.* **2003**, *9*, 1991. (e) Barlow, S.; Marder, S. R. *Chem. Commun.* **2000**, 1555. (f) Jen, A. K.-Y.; Ma, H.; Wu, X.; Wu, J.; Liu, S.; Marder, S. R.; Dalton, L. R.; Shu, C.-F. *SPIE Proc.* **1999**, *3623*, 112.

(5) (a) Qudar, J. L.; Chemla, D. S. *J. Chem. Phys.* **1977**, *66*, 2664. (b) Marder, S. R.; Beratan, D. N.; Cheng, L.-T. *Science* **1991**, *252*, 103.

(6) (a) Marder, S. R.; Kippelen, B.; Jen, A. K.-Y.; Peyghambarian, N. *Nature* **1997**, *388*, 845. (b) Marder, S. R.; Cheng, L. T.; Tiemann, B. G.; Friedli, A. C.; Blanchard-Desce, M.; Perry, J. W.; Skindhoej, J. *Science* **1994**, *263*, 511. (c) Marder, S. R.; Gorman, C. B.; Tiemann, B. G.; Cheng, L. T. *J. Am. Chem. Soc.* **1993**, *115*, 2524.

(7) (a) Albert, I. D. L.; Marks, T. J.; Ratner, M. A. *Chem. Mater.* **1998**, *10*, 753. (b) Albert, I. D. L.; Marks, T. J.; Ratner, M. A. *J. Am. Chem. Soc.* **1997**, *119*, 6575. (c) Rao, V. P.; Jen, A. K.-Y.; Chandrasekhar, J.; Namboothiri, I. N. N.; Rathna A. *J. Am. Chem. Soc.* **1996**, *118*, 12443.

(8) Galvan-Gonzalez, A.; Belfield, K. D.; Stegeman, G. I.; Canva, M.; Marder, S. R.; Staub, K.; Levina, G.; Twieg, R. J. *J. Appl. Phys.* **2003**, *94*, 756 and references therein.

(9) (a) Traber, B.; Wolff, J. J.; Rominger, F.; Oeser, T.; Gleiter, R.; Goebel, M.; Wortmann, R. *Chem. Eur. J.* **2004**, *10*, 1227. (b) Zhu, P.; Yang, Y.; Facchetti, A.; Marks, T. J. *J. Am. Chem. Soc.* **2004**, *126*, 15974. (c) Wortmann, R.; Lebus-Henn, S.; Reis, H.; Papadopoulos, M. G. *THEOCHEM* **2003**, *633*, 217. (d) Yang M.-L.; Champagne, B. *J. Phys. Chem. A* **2003**, *107*, 3942. (e) Ostroverkhov, V.; Petschek, R. G.; Singer, K. D.; Twieg, R. J. *Chem. Phys. Lett.* **2001**, *340*, 109. (f) Wolff, J. J.; Segler, F.; Matschiner, R.; Wortmann, R. *Angew. Chem., Int. Ed. Engl.* **2000**, *39*, 1436. (g) Van, Elshocht, S.; Verbiest, T.; Kauranen, M.; Ma, L.; Cheng, H.; Musick, K.; Pu, L.; Persoons, A. *Chem. Phys. Lett.* **1999**, *309*, 315. (h) Brasselet, S.; Cherioux, F.; Audebert, P.; Zyss, J. *Chem. Mater.* **1999**, *11*, 1915. (i) Lee, Y.-K.; Jeon, S.-J.; Cho, M. *J. Am. Chem. Soc.* **1998**, *120*, 10921. (j) Wortmann, R.; Glania, C.; Krämer, P.; Matschiner, R.; Wolff, J.; Kraft, S.; Treptow, B.; Barbu, E.; Längle, D.; Görlitz, G. *Chem. Eur. J.* **1997**, *3*, 1765. (k) Moylan, C. R.; Ermer, S.; Lovejoy, S. M.; McComb, I.-H.; Leung, D. S.; Wortmann, R.; Krdmer P.; Twieg, R. J. *J. Am. Chem. Soc.* **1996**, *118*, 8, 12950.

(10) (a) Kay, A. J.; Woolhouse, A. D.; Zhao, Y.; Clays, K. *J. Mater. Chem.* **2004**, *14*, 1321. (b) Innocenzi, P.; Miorin, E.; Brusatin, G.; Abbotto, A.; Beverina, L.; Pagani, G. A.; Casalboni, M.; Sarcinelli, F.; Pizzoferrato, R. *Chem. Mater.* **2002**, *14*, 3758. (c) Kay, A. J.; Woolhouse, A. D.; Gainsford, G. J.; Haskell, T. G.; Barnes, T. H. *J. Mater. Chem.* **2001**, *11*, 996. (d) Fort, A.; Mager, L.; Muller, J.; Combellas, C.; Mathey, G.; Thiébault, A. *Opt. Mater.* **1999**, *12*, 339. (e) Szablewski, M.; Thomas, P. R.; Thornton, A.; Bloor, D.; Cross, G. H.; Cole, J. M.; Howard, J. A. K.; Malagoli, M.; Meyer, F.; Bredas, J. L.; Wenseleers, W.; Goovaerts, E. *J. Am. Chem. Soc.* **1997**, *119*, 3144.

Chart 1

TICTOID Chromophores

Chart 2

TM

TM-1, n = 0, R = Me

TM-2, n = 1, R = *n*-Octyl

TMC

TMC-1, n = 0, R = Me

TMC-2, n = 0, R =

TMC-3, n = 1, R =
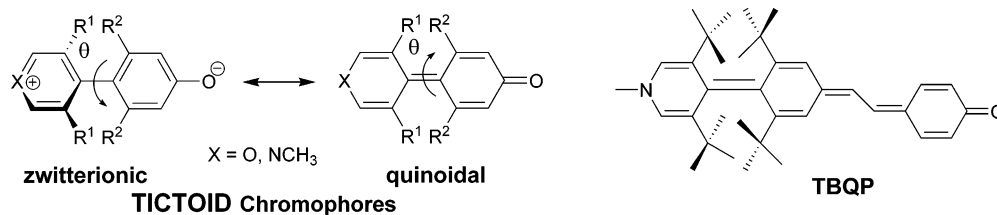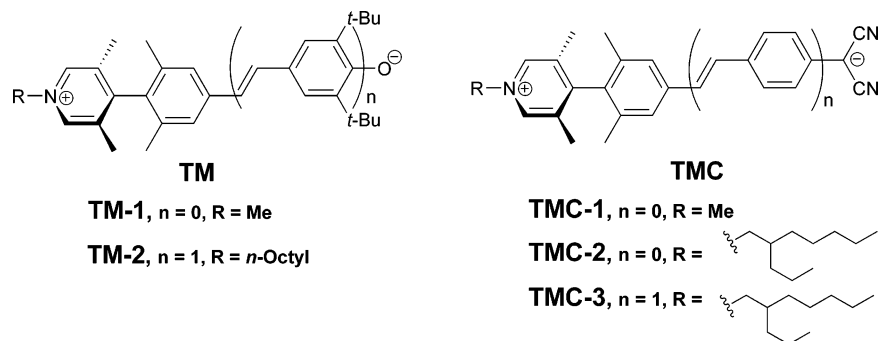
completely new insights.[11] Alternative paradigms for very large β chromophores would clearly be desirable, and there is growing evidence that simple two-state systems are inadequate.[12]

Twisted intramolecular charge-transfer (TICT) molecules have received significant attention in the quest to understand their nonlinear optical response.[13] In the TICT response mechanism, rotation about a bond connecting conjugated D/A substituents can reduce the overlap between the orbitals of the D/A groups, providing a means by which nearly complete electron transfer can occur upon optical excitation,[14] strongly enhancing CT interactions and leading to large hyperpolarizabilities. Recent theoretical work in this laboratory[15] suggests that molecules with *twisted* π-electron systems bridging D and A substituents (TICTOID; Chart 1) might exhibit unprecedentedly large hyperpolarizabilities. Such chromophores could have relatively simple zwitterionic biaryl structures in which β_{zzz} and the linear optical response are sterically tunable via R^1, R^2 modification of the interplanar dihedral angle (θ). Maximum β magnitudes are predicted at $\theta \approx 70-85°$,[15] with twist-induced reduction in D−π−A conjugation leading to aromatic stabilization and formal charge-separated zwitterionic ground states, relatively low-energy optical excitations, and large dipole moment changes from the ground to first excited state. For example, the maximum nonresonant $\mu\beta$ estimated for a tetra-*tert*-butyl-substituted 4-quinopran (**TBQP**) with a full AM1-optimized interplanar dihedral angle of 104° is ~70 000 × 10^{-48} esu at 0.1 eV.[15] Molecules with small numbers of π electrons

could thereby exhibit far larger βs than conventional planar π chromophores and, in principle, be as simple as two connected arene rings, hence less susceptible to thermal/oxidative/photochemical degradation. Notably, the mechanism of the response to the light field here is distinctly different from the current BLA/two-state models, suggesting a promising new strategy for ultrahigh response EO chromophores.

In recent communications[16] we briefly described the first synthetic realization of *twisted* π-electron system chromophores (tictoids). Those preliminary reports described initial synthetic approaches, aggregation tendencies in solution, and evidence of unprecedented molecular hyperpolarizabilities, in turn raising a number of intriguing questions. In the present contribution, we disclose full details and discussion of synthetic approaches, structural characteristics, aggregation properties, and the exceptional NLO/EO properties of this unconventional tictoid chromophore family (**TM** and **TMC**; Chart 2), investigated using a full battery of experimental techniques, including condensed state X-ray diffraction, solution-phase NOE NMR, and optical/IR/^{13}C NMR spectroscopic studies in both the solution phase and the solid state, electrochemistry, concentration-dependent optical and fluorescence spectroscopy, pulsed field gradient spin−echo (PGSE) NMR spectroscopy, solution-phase DC electric-field-induced second-harmonic generation (EFISH) spectroscopy, and Teng−Man electro-optic measurements, combined with high-level state-averaged complete active space self-consistent field (SA-CASSCF) computational approaches. The results include molecular hyperpolarizabilities as large as 15× greater than ever previously reported ($\mu\beta$ as high as −488 000 × 10^{-48} esu at 1907 nm) and poled polymers with EO responses 3−5× greater than reported heretofore in the open literature[3] (r_{33} as high as 330 pm/V at 1310 nm). Thus, we suggest new paradigms for molecular hyperpolarizability and organic electro-optics.

(11) (a) Tripathy, K.; Moreno, J. P.; Kuzyk, M. G.; Coe, B. J.; Clays, K.; Kelley, A. M. *J. Chem. Phys.* **2004**, *121*, 7932. (b) Kuzyk, M. G. *Phys. Rev. Lett.* **2000**, *85* (6), 1218.

(12) (a) Di Bella, S. *New J. Chem.* **2002**, *26*, 495. (b) Meshulam, G.; Berkovic, G.; Kotler, Z. *Opt. Lett.* **2001**, *26*, 30. (c) Brasselet, S.; Zyss, J. *J. Nonlinear Opt. Phys. Mater.* **1996**, *5*, 671. (d) Ledoux, I.; Zyss, J. *Pure Appl. Opt.* **1996**, *5*, 603.

(13) (a) Sen, R.; Majumdar, D.; Battacharyya, S. P.; Battacharyya, S. N. *J. Phys. Chem.* **1993**, *97*, 7491. (b) Lippert, E.; Rettig, W.; Bonačić-Koutecký, V.; Heisel, F.; Mihe, J. A. *Adv. Chem. Phys.* **1987**, *68*, 1.

(14) Rettig, W. *Appl. Phys. B* **1988**, *45*, 145.

(15) (a) Keinan, S.; Zojer, E.; Bredas, J.-L.; Ratner, M. A.; Marks, T. J. *THEOCHEM* **2003**, *633* (2−3), 227. (b) Albert, I. D. L.; Marks, T. J.; Ratner, M. A. *J. Am. Chem. Soc.* **1998**, *120*, 11174. (c) Albert, I. D. L.; Marks, T. J.; Ratner, M. A. *J. Am. Chem. Soc.* **1997**, *119*, 3155.

(16) (a) Kang, H.; Facchetti, A.; Stern, C. L.; Rheingold, A. L.; Kassel, W. S.; Marks, T. J. *Org. Lett.* **2005**, *7*, 3721. (b) Kang, H.; Facchetti, A.; Zhu, P.; Jiang, H.; Yang, Y.; Cariati, E.; Righetto, S.; Ugo, R.; Zuccaccia, C.; Macchioni, A.; Stern, C. L.; Liu, Z.; Ho, S.-T.; Marks, T. J. *Angew. Chem., Int. Ed.* **2005**, *44*, 7922.

Experimental Section

Materials and Methods. All reagents were purchased from Aldrich Chemical Co. and used as received unless otherwise indicated. THF was distilled from sodium/benzophenone and methylene chloride from CaCl$_2$. Chloroform was dried and distilled from anhydrous K$_2$CO$_3$. Toluene was dried by passing through two packed columns of activated alumina and Q5 under N$_2$ pressure and regularly tested with benzophenone ketyl in ether solution. The reagent 1-iodo-4-vinyl-benzene was purchased from Karl Industries Inc. and 2-propyl-1-heptanol from Narchem Co. The reagents 4-bromo-3,5-dimethyl-pyridine 1-oxide (**1**)[17] and ligand dicyclohexyl-(2-phenanthren-9-yl-phenyl)-phosphine (**DCP-PP**) for catalytic Suzuki coupling were synthesized according to literature procedures.[18] Solution NMR spectra were recorded on a Varian Mercury 400 MHz or Varian INOVA 500 MHz spectrometer except for NOE and PGSE measurements (see below). Solid-state ^{13}C CPMAS NMR spectra were recorded on a Varian VXR-500 MHz spectrometer at room temperature with a spinning rate of 10 kHz using a 3.2 mm zirconia rotor with Aurum caps. The cross-polarization contact time was 4.0 ms, and the repetition time was 5.0 s. Mass spectra were recorded on a Micromass Quattro II Triple Quadrupole HPLC/MS/MS mass spectrometer. Elemental analyses were performed by Midwest Microlabs. Optical spectra were recorded on a Cary 5000 spectrophotometer. Emission spectra were recorded on a PTI QM2 Fluorescence Instrument. Thermal analysis was performed with a TA Instruments SDT 2960 simultaneous DTA-TGA instrument under N$_2$ at 1.0 atm. The temperature ramp rate was 1.5 °C/min. IR spectra were obtained on a Bio-Rad FTS-40 FTIR spectrometer. Cyclic voltammetry was performed with a BAS 100 electrochemical analyzer using a three-electrode cell (carbon working electrode, Ag wire pseudo-reference electrode, and Pt wire counter electrode) with 0.1 M Bu$_4$NPF$_6$ in anhydrous CH$_3$CN as the electrolyte. All potentials are quoted vs the ferrocene/ferrocenium (Fc/Fc$^+$) couple internal standard. Synthetic procedures and characterization are reported in the Supporting Information.

Single-Crystal X-ray Diffraction. All diffraction measurements were carried out on a Bruker SMART CCD diffractometer with graphite-monochromated MoKα (0.71073 Å) radiation. Data were collected using the Bruker SMART detector, processed using the SAINT-NT package from Bruker, and corrected for Lorentz and polarization effects. The structures were solved by direct methods (SHELXTL-90) and expanded using Fourier techniques (SHELXTL-97). The non-hydrogen atoms were refined anisotropically. Hydrogen atoms on water molecules of solvation were refined with group isotropic displacement parameters. The remaining hydrogen atoms were included in idealized positions but not refined. All calculations were performed using the Bruker SHELXTL9 crystallographic software package. Crystallographic data are summarized in Table S1.

NOE Measurements of Twist Angle in Solution. A sample of **TMC-2** in dry DMSO (dried and stored over activated molecular sieves) was degassed via four freeze−pump−thaw cycles. NOE measurements were performed on a Bruker Avance spectrometer operating at 400.13 MHz using the 1D-GOESY pulse sequence of Keeler and co-workers[19] under the initial rate approximation.[20] The singlet relative to H(3) was inverted, and NOEs were measured on both H(4) and H(2) as a function of temperature (294−342 K).
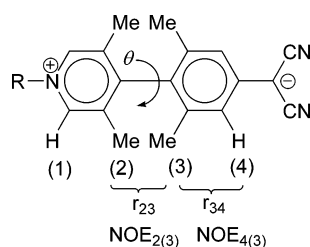
Under the initial rate approximation, the NOE build-up is only proportional to the cross relaxation rate constant σ_{IS} according to eq 2

$$\frac{d(NOE_I\{S\})}{d\tau}\Big|_{\tau=0} = 2\sigma_{IS} \tag{2}$$

σ_{IS} can be expressed in terms of internuclear distance r_{IS} and correlation time τ_c according to eq 3

$$\sigma_{IS} = \left(\frac{\mu_0}{4\pi}\right)^2 \frac{\hbar^2 \gamma_I^2 \gamma_S^2}{10} \left(\frac{6\tau_C}{1+(\omega_I+\omega_S)^2\tau_C^2} - \frac{\tau_C}{1+(\omega_I-\omega_S)^2\tau_C^2}\right) r_{IS}^{-6} \tag{3}$$

τ_C varies with temperature according to the following eq 4[21]

$$\tau_C = \tau^0 \cdot e^{E_R/kT} \tag{4}$$

where E_R is the activation energy for rotational reorientation, τ^0 is a constant, and k is the Boltzmann constant. For a homonuclear experiment, combining eqs 3 and 4 affords eq 5, where the temperature dependence of σ_{IS} is explicit

$$\sigma_{IS} = \left(\frac{\mu_0}{4\pi}\right)^2 \frac{\hbar^2 \gamma_I^2 \gamma_S^2}{10} \cdot \tau^0 \cdot e^{E_R/kT} \left(\frac{6}{1+(2\omega)^2(\tau^0 \cdot e^{E_R/kT})^2} - 1\right) r_{IS}^{-6} \tag{5}$$

Equation 5 was used to fit the experimental σ_{IS} values (Table S2). The fitting results provide the corresponding r_{IS}, E_R, and τ^0.[22] Despite the goodness of the fits, the error on the derived r_{IS} values was estimated to be ca. 5%, corresponding to an uncertainty of ±0.1−0.2 Å.[22] The experimentally determined r_{23} distance was incremented by 10% to account for the known overestimation of short distances when conformational averaging, aryl liberation in this case, is present (see ref 20, pp 171−173). Comparison between the obtained r_{23} and the computed r_{23} distance for seven static conformations, having a dihedral angle of 89.6°, 84.4°, 80.0°, 75.2°, 69.6°, 64.4°, and 59.6° allows the average dihedral twist angle between the two aryl rings in solution to be estimated.

Pulsed Field Gradient Spin−Echo (PGSE) NMR Spectroscopy. ^{1}H PGSE NMR measurements were performed using the standard stimulated echo pulse sequence[23] on a Bruker AVANCE DRX 400 spectrometer equipped with a GREAT 1/10 gradient unit and a QNP probe with a Z-gradient coil at 295.7 K without spinning. The shape of the gradients was rectangular, their duration (δ) was 4 ms, and their strength (G) was varied during the experiments. All spectra were acquired using 32K points and a spectral width of 5000 Hz and processed with a line broadening of 1.0 Hz. The semilogarithmic plots of $\ln(I/I_0)$ vs G^2 were fit using a standard linear regression algorithm; the R factor was always greater than 0.99. Different values of "nt" (number of transients) and number of different gradient strengths (G) were used for different samples, depending on solution viscosity and solute concentration. The two **TMC** ortho methyl group resonances

(17) Klán, P. *Monatsh. Chem.* **1993**, *124*, 327.
(18) Yin, J.; Rainka, M. P.; Zhang, X.-X.; Buchwald, S. L. *J. Am. Chem. Soc.* **2002**, *124*, 1162.
(19) Stonehouse, J.; Adell, P.; Keeler, J.; Shaka, A. J. *J. Am. Chem. Soc.* **1994**, *116*, 6037.
(20) The mixing time (τ_m) was set to 150 ms as a good compromise between initial rate approximation (τ_m < 5 times the shorter T_1) and a sufficient signal to noise ratio. Neuhaus, D.; Williamson M. *The Nuclear Overhauser Effect in Structural and Conformational Analysis*; VCH Publishers: New York, 1989.
(21) (a) Doddrell, D. M.; Bendall, M. R.; O'Connor, A. J.; Pegg, D. T. *Aust. J. Chem.* **1977**, *30*, 943. (b) Farrar, T. C.; Becker, E. D. *Pulse and Fourier Transform N.M.R.*; Academic Press: New York, 1971.
(22) Zuccaccia, C.; Bellachioma, G.; Cardaci, G.; Macchioni, A. *J. Am. Chem. Soc.* **2001**, *123*, 11020.
(23) Tanner, J. *J. Chem. Phys.* **1970**, *52*, 2523−2526.

(one from each ring) were used for the analysis. The dependence of the resonance intensity (I) on a constant diffusion time and on a varied gradient strength (G) is described by eq 6

$$\ln \frac{I}{I_0} = -(\gamma\delta)^2 D_t\left(\Delta - \frac{\delta}{3}\right)G^2 \tag{6}$$

where I = intensity of the observed spin echo, I_0 = intensity of the spin echo without gradients, D_t = diffusion coefficient, Δ = delay between the midpoints of the gradients, δ = length of the gradient pulse, and γ = magnetogyric ratio. For pure solvents, the diffusion coefficient D_t, which is directly proportional to the slope of the regression line obtained by plotting $\log(I/I_0)$ vs G^2, was estimated by measuring the proportionality constant using an HDO sample (0.04%) in D_2O (known diffusion coefficient in the range 274–318 K)[24] under the exact same conditions as the sample of interest [D_t(CD_2Cl_2) = 33.2 $\times 10^{-10}$ m^2 s^{-1}, D_t(DMSO-d_6) = 6.5 $\times 10^{-10}$ m^2 s^{-1}]. Residual solvent signals were then used as internal standards to account for systematic changes in solution viscosity (i.e., the reported D_t values refer to a hypothetical experiment carried out in a solution having the nominal reported concentration but the viscosity of the pure solvent at that temperature)[25] or random changes in the actual probe temperature as well as gradient strength reproducibility.[26]

PGSE measurements were carried out for **TMC-2** and **TMC-3** in CD_2Cl_2 and DMSO-d_6 over a range of concentrations. Hydrodynamic radii of the diffusing particles (r_H) were derived from the experimentally determined D_t data using the Stokes–Einstein equation

$$D_t = \frac{kT}{6\pi\eta r_H\left(\frac{f}{f_0}\right)} \tag{7}$$

where k is the Boltzmann constant, T is the temperature, and η is the solution viscosity. The f/f_0 ratio is introduced to take into account the ellipsoidal shapes of **TMC-2** and **TMC-3**, where f is the frictional coefficient of the ellipsoid and f_0 is that of a sphere having an equal volume.[27] The f/f_0 ratio depends on the shape (prolate or oblate) and ratio of the major (a) to minor (b) axis of the ellipsoid. For prolate ellipsoid-like **TMC-2**, $a/b \approx 2.9$ and $f/f_0 \approx 1.1$, while for **TMC-3**, $a/b \approx 4.1$ and $f/f_0 \approx 1.2$.[27] From the hydrodynamic radii obtained, the hydrodynamic volumes (V_H) of the diffusing chromophores were calculated and then compared with the van der Waals volumes (V_{vdW}) obtained from crystallographic data or molecular modeling. The V_H/V_{vdW} ratio represents the aggregation number (N), similar to that defined by Pochapsky,[28] and is useful in comparing trends over a range of concentrations.

EFISH Measurements. Measurements of $\mu\beta$, the products of the chromophore dipole moment (μ) and the projection of β_{VEC}, the vector part of the molecular first-order hyperpolarizability β tensor along the

direction of μ, were performed by solution-phase DC electric-field-induced second-harmonic (EFISH) generation methods,[29] which provide direct information on the intrinsic molecular NLO response via eq 8

$$\gamma_{EFISH} = (\mu\beta/5kT) + \gamma(-2\omega;\omega,\omega,0) \tag{8}$$

where $\mu\beta/5kT$ is the dipolar orientational contribution and $\gamma(-2\omega; \omega, \omega, 0)$, a third-order term at frequency ω of the incident light, is the electronic contribution to γ_{EFISH}, which is negligible for molecules of the type investigated here.[30]

EFISH measurements were carried out in CH_2Cl_2 and DMF solutions over a broad range of concentrations (10^{-4}–10^{-6} M) at a nonresonant fundamental wavelength of 1907 nm using a Q-switched, mode-locked Nd^{3+}:YAG laser [pulse durations of 15 ns (90 ns) at a 10 Hz repetition rate]. The 1064 nm initial wavelength was shifted to 1907 nm by a Raman shifter with a high-pressure H_2 cell. Solutions were prepared under N_2. CH_2Cl_2 was freshly distilled from $CaCl_2$. The organic base 1,4-diaza-bicyclo[2.2.2]octane (DABCO) (molar ratio DABCO/chromophore equal to 0.5/1.0) was added to the solutions to increase chromophore stability. The $\mu\beta$ values reported (Table S3) are the averages of 16 successive measurements performed on each sample. The standard deviation was never greater than 22%.

In Situ Poling and Direct Electrooptic Measurements on TMC-Containing Guest–Host Polymer Thin Films. The effective electro-optic coefficient, r_{33}, of poled **TMC**-based guest–host materials was measured using the Teng–Man reflection technique.[31] Figure S1 shows a schematic diagram of the in situ poling and direct Teng–Man EO measurement setup. A 633 nm He–Ne laser is used for alignment of optical components, and a CW diode laser at 1310 nm (TEC) is used as the working laser source. The laser beam (1310 nm) travels through a polarizer, where the orientation is set at 45° with respect to the laser incident plane, then passes through the transparent conducting oxide (TCO) top electrode, and then the EO-active thin film before being reflected by the bottom gold electrode. The reflected laser beam travels through a compensator and then an analyzer, which is cross-polarized with respect to the polarizer. The signals are collected by a detector and then monitored with an oscilloscope and lock-in amplifier. Apertures are used for collimation purposes. The sample is mounted under an N_2 flow on a temperature-controlled heated stage with good thermal contact. An AC modulation voltage, amplifying the input signal from a signal generator, is applied to the sample with a frequency of 1 kHz, with the amplitude ranging from 1.0 to 10 V. A DC bias generated by the high-voltage amplifier is applied to the sample, with a microamp meter monitoring the poling current ($\sim$10 μA). In the present experiments, assuming $r_{33} = 3r_{13}$, r_{33} is derived from eq 9[32]

$$r_{33} = \frac{3\sqrt{2}}{4}\frac{\lambda}{\pi}\frac{1}{V_M}\frac{V_{AC}}{V_{DC}}\frac{\sqrt{n^2 - \sin^2\theta}}{n^2\sin^2\theta} \tag{9}$$

where λ is the wavelength of the laser, V_{DC} is the working voltage, V_{AC} is the modulated signal, V_M is the modulation voltage applied to the sample, θ is the incident angle of the laser beam (fixed at 45°), and n is the refractive index of the thin film.

The EO measurement sample has the structure glass substrate/TCO/ EO thin film/Au (Figure S1). The TCO electrode (NIR transparent In_2O_3), having a thickness around 160 nm and a conductivity of 100 S/cm, was grown on Eagle 2000 glass substrates at room temperature by ion-assisted deposition (IAD).[31c] **TMC** guest–host thin films ($\sim$1

(24) Mills, R. *J. Phys. Chem.* **1973**, *77*, 685. Data at different temperatures were estimated by interpolation of the data reported by Mills, giving $D_{HDO} = 1.780 \times 10^{-9}$ m^2 s^{-1} at 295.7 K.

(25) (a) The viscosity of CD_2Cl_2 was estimated to be 0.4256 cp at 295.7 K by interpolation of the data reported for CH_2Cl_2 (*CRC Handbook of Chemistry and Physics*, 67th ed.; Weast, R. C., Ed.; Chemical Rubber: Cleveland, 1986) and corrected for the reduced mass as proposed by Holz et al. (Holz, M.; Mao, X.; Seiferling, D.; Sacco, A. *J. Chem. Phys.* **1996**, *104*, 669). (b) The viscosity of DMSO-d_6 was estimated to be 2.138 cp at 295.7 K by interpolation of the data reported for DMSO (Higashigaki, Y.; Christensen, D. H.; Wang, C. H. *J. Phys. Chem.* **1981**, *85*, 2531) and corrected for the reduced mass as proposed by Holz et al. (Holz, M.; Mao, X.; Seiferling, D.; Sacco, A. *J. Chem. Phys.* **1996**, *104*, 669).

(26) (a) Zuccaccia, D.; Macchioni, A. *Organometallics* **2005**, *24*, 3476. (b) Zuccaccia, C.; Stahl, N. G.; Macchioni, A.; Chen, M. C.; Roberts, J. A.; Marks, T. J. *J. Am. Chem. Soc.* **2004**, *126*, 1448.

(27) Perrin, F. *J. Phys. Radium* **1936**, *7*, 1.

(28) (a) Mo, H.; Pochapsky, C. T. *J. Phys. Chem. B* **1997**, *101*, 4485. (b) Pochapsky, S. S.; Mo, H.; Pochapsky, C. T. *J. Chem. Soc., Chem. Commun.* **1995**, 2513.

(29) (a) Levine, B. F.; Bethea, C. G. *Appl. Phys. Lett.* **1974**, *24*, 445. (b) Singer, K. D.; Garito, A. F. *J. Chem. Phys.* **1981**, *75*, 3572. (c) Ledoux, I.; Zyss, J. *Chem. Phys.* **1982**, *73*, 203.

(30) (a) Kanis, D. R.; Lacroix, P. G.; Ratner, M. A.; Marks, T. J. *J. Am. Chem. Soc.* **1994**, *116*, 10089. (b) Roberto, D.; Ugo, R.; Bruni, S.; Cariati, E.; Cariati, F.; Fantucci, P.; Invernizzi, I.; Quici, S.; Ledoux, I.; Zyss, J. *Organometallics* **2000**, *19*, 1775. (c) Lesley, M. J. G.; Woodward, A.; Taylor, N. J.; Marder, T. B.; Cazenobe, I.; Ledoux, I.; Zyss, J.; Thornton, A.; Bruce, D. W.; Kakkar, A. K. *Chem. Mater.* **1998**, *10*, 1355.

(31) (a) Teng, C. C.; Man, H. T. *Appl. Phys. Lett.* **1990**, *56* (18), 1734. (b) Schildkraut, J. S. *Appl. Opt.* **1990**, *29*, 2839. (c) Wang, L.; Yang, Y.; Marks, T. J.; Liu, Z.; Ho, S.-T. *Appl. Phys. Lett.* **2005**, *87* (16), 161107/1.

(32) Shuto, Y.; Amano, M. *J. Appl. Phys.* **1995**, *77*, 4632.

μm) were prepared by spin-coating onto the TCO substrate a solution of **TMC**/host polymer in DMF at 1000 rpm for 60 s and curing the resulting film at 110 °C in a vacuum oven (60 mTorr) for 16 h. The bottom Au electrode (~150 nm) was then deposited on the **TMC** guest–host thin films by e-beam evaporation techniques.

Computational Methodology. The model compound **TM-1′** was used as an analog of chromophore **TM-1** to reduce the computational demands. All electronic structure calculations were performed using the MOLCAS quantum chemistry package[33] with the 6-31G** basis set.[34] All geometries were optimized with respect to the ground-state wave function at a particular geometry where the ring–ring dihedral twist angle had been fixed. For twist angles between 50° and 90°, excitation energies were obtained with a three-state state-average complete active space (SA-CASSCF) level of theory with four π electrons in three π molecular orbitals. At the 90° geometry, the lowest three states converged to a ground-state Ψ_D, the first excited state Ψ_Z (notationally D and Z represent diradical and zwitterion states, respectively), and the second excited state, which can be thought of as an $n \rightarrow \pi$* transition ($\Psi_{n \rightarrow \pi*}$). In order to account for the effects of dynamical electron correlation, CASPT2 single-point energy calculations were performed at the CASSCF geometry. The CASPT2 and CASSCF results differ by no more than 0.1 eV in all of these calculations; therefore, the CASSCF active space is adequate for the purpose of describing the differences in computed quantities.

TM-1'
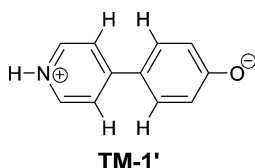
Instead of explicitly including the four *ortho*-methyl groups of **TM-1** in state-average calculations, a model methyl-repulsion potential was derived by subtracting the energy of the ground state of **TM-1′** as a function of twist angle from the ground-state torsional potential of **TM-1′**. The model methyl-repulsion potential was then shifted so that its potential energy is zero at the 90° geometry, where the *ortho*-methyl groups interact the least. This methyl-repulsion potential was added to the ground- and excited-state energies from the three-state SA-CASSCF calculations. Finally, the SA-CASSCF calculations were slightly shifted by 0.3 eV so that the energy difference matched that of the higher-quality single-state-CASSCF(14,13) calculations at the 90° geometry. Considering that nonlinear response depends on the difference in state energies, these electronic states were characterized by describing their composition in terms of the frontier molecular orbitals at the highly symmetric (C_{2v}) twisted geometry. Each state was classified after inspecting its CI coefficients, molecular orbitals, and dipole moment.

Results

The synthesis of a new series of tictoid chromophores is first reported. Of particular interest here are the enforced dihedral twist angles and related structural characteristics that define the architectures of these zwitterions. To this end, single-crystal X-ray diffraction structure determinations are performed on a number of the target chromophores as well as on their synthetic precursors (including neutral, positively charged, and zwitterionic molecules) to provide structural information in the solid state. It will be seen that the present tetra-*ortho*-methylbiaryl substitution pattern indeed enforces very large and uniform twist

angles across the series and that these tictoid chromophores possess highly charge-separated zwitterionic ground states in the solid state. Molecular properties and structural characteristics in solution are then studied by a combination of techniques, including NOE NMR, optical absorption (UV–vis) spectroscopy, fluorescence spectroscopy, cyclic voltammetry, and infrared (IR) vibrational spectroscopy. It is further shown that the dihedral twist angle and structural characteristics observed in the solid state persist in the solution phase by NOE-derived dihedral twist angle measurements in solution and comparative solid-state vs solution ^{13}C NMR, IR, and optical spectroscopic analysis. To understand in depth how aggregation of these highly dipolar zwitterions may affect chromophore measured linear/nonlinear optical properties, the solution-phase molecularity is fully investigated using several complementary experimental techniques, including concentration-dependent optical absorption, fluorescence, and pulsed field gradient spin–echo (PGSE) NMR spectroscopies, in comparison with the solid-state X-ray diffraction data. These studies provide clear evidence for the formation of centrosymmetric aggregates at high concentrations in nonpolar solvents and in the condensed state and provide quantitative information on the state of aggregation. Molecular hyperpolarizabilities are then evaluated by the solution-phase DC electric-field-induced second-harmonic generation (EFISH) methods, and the electro-optic coefficients (r_{33}) of poled host–guest polymers containing these chromophores are directly measured by Teng–Man reflection techniques. Aggregation effects on these measurements are also taken into account and discussed. Finally, high-level computations provide a rationale for the observed exceptional hyperpolarizabilities in these twisted chromophores and demonstrate significant solvation effects on hyperpolarizabilities, in good agreement with experiment.

Chromophore Synthetic Approaches. The syntheses of the present new families of tictoid chromophores are summarized in Scheme 1. The highly encumbered asymmetric tetra-*ortho*-methylbiaryl core **3** was constructed via Suzuki cross-coupling of hindered 4-bromopyridine *N*-oxide **1** and phenyl boronic acid **2** using a Pd/dicyclohexyl-(2-phenanthren-9-yl-phenyl)-phosphane (**DCPPP**) catalyst.[18] Pyridine *N*-oxide **3** was next reduced to pyridine **4** in a facile and quantitative fashion using Pd-catalyzed hydrogenation with sodium hypophosphite as the hydrogen source.[35] Subsequent cleavage of the **4** methoxyl group with pyridine + HCl affords pyridylphenol intermediate **6.** This product was then quaternized with methyl iodide and deprotonated with sodium methoxide to afford chromophore **TM-1.** *N*-Methylpyridinium salts **5** and **7** were also prepared for X-ray diffraction studies.

The crucial synthetic biaryl iodide intermediate **11** was prepared via a four-step phenol-to-aryl iodide conversion. Phenol **6** was first converted to triflate **8**. Next, Pd-catalyzed coupling[36] of triflate **8** with benzophenone imine leads to diphenyl ketimine **9** in 98% yield. Subsequent quantitative hydrolysis of **9** to primary aniline **10** was achieved using hydroxylamine hydrochloride. Biaryl iodide **11** was then obtained via diazotization of **10** and iodination of the corresponding diazonium salt with NaI. Chromophore **TM-2** was synthesized via conventional Heck cross-coupling of **11** and styrenic coupling partner **12**,
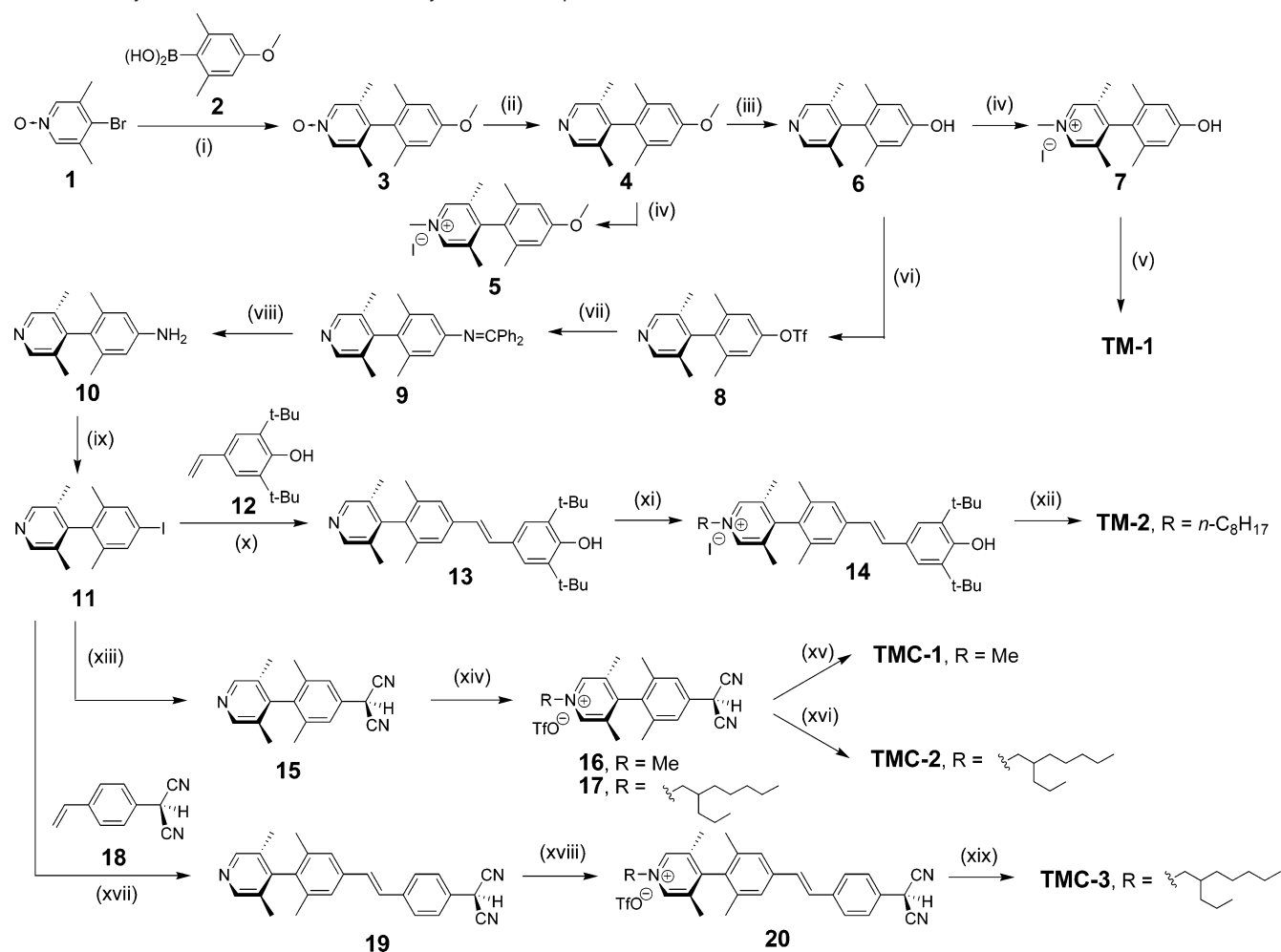
(33) Karlström G.; Lindh R.; Malmqvist , P.-Å.; Roos, B. O.; Ryde, U.; Veryazov, V.; Widmark, P.-O.; Cossi , M.; Schimmelpfennig, B.; Neogrady, P.; Seijo, L. *Comput. Mater. Sci.* **2003**, *28*, 222.
(34) (a) Hehre, W. J.; Ditchfield, R.; Pople, J. A. *J. Chem. Phys.* **1972**, *56*, 2257. (b) Hariharan, P. C.; Pople, J. A. *Theor. Chim. Acta* **1973**, *28*, 213.

(35) Balicki, R.; Kaczmarek, L. *Gazz. Chim. Ital.* **1994**, *124* (9), 385.
(36) Wolfe, J. P.; Åhman, J.; Sadighi, J. P.; Singer, R. A.; Buchwald, S. L. *Tetrahedron Lett.* **1997**, *38*, 6367.

Scheme 1. Synthesis of Twisted π-Electron System Chromophrores[a]

[a] (i) Pd₂(dba)₃/DCPPP, K₃PO₄, toluene; (ii) NaH₂PO₂, Pd/C, AcOH; (iii) pyridine + HCl; (iv) MeI; (v) MeONa, MeOH; (vi)Tf₂O, pyridine; (vii) NH=CPh₂, Pd(OAc)₂/BINAP, Cs₂CO₃, THF; (viii) NH₂OHHCl, NaOAc, MeOH; (ix) NO⁺BF₄⁻, CH₃CN, NaI; (x) Pd(OAc)₂/PPh₃, Et₃N; (xi) n-C₈H₁₇I, CH₂Cl₂; (xii) MeONa, MeOH; (xiii) NaCH(CN)₂, Pd(PPh₃)₄, DME; (xiv) ROTf, CH₂Cl₂; (xv) aq. NaOH (xvi) MeONa, MeOH; (xvii) Pd(OAc)₂/PPh₃, Et₃N, DMF; (xviii) ROTf, CH₂Cl₂; (xix) MeONa, MeOH.

which was readily obtained via thermal decarboxylation of 3,5-di-*tert*-butyl-4-hydroxycinnamic acid in DMF. The resulting stilbene precursor **13** was quaternized with *n*-octyl iodide and then deprotonated with sodium methoxide to afford chromophore **TM-2** in 87% yield.

Pd-catalyzed coupling of **11** with sodium dicyanomethanide affords **15** in high yield (96%), which is next regioselectively *N*-quaternized[37] with alkyl triflates and then deprotonated to afford chromophores **TMC-1** (80% yield) and **TMC-2** (67% yield). Styrene precursor **18** was synthesized via Pd-catalyzed coupling of 1-iodo-4-vinyl-benzene with sodium dicyanomethanide in 72% yield. Subsequent Heck coupling of **11** with styrene **18** affords chromophore precursor **19** in 55% yield. This intermediate was alkylated and then deprotonated to afford chromophore **TMC-3** in 66% yield. All new compounds have been fully characterized via conventional analytical/spectroscopic techniques, including multinuclear NMR spectroscopy, mass spectrometry, and elemental analysis.

Condensed-State Structural Chemistry. X-ray diffraction structural analyses were performed on neutral synthetic inter-

mediates **3** and **6**, *N*-methyl pyridinium salts **5** and **7**, and tictoid chromophores **TM-1**, **TM-2**, **TMC-1**, and **TMC-2**. Single crystals were obtained via slow evaporation of saturated solutions. Important crystallographic data for these compounds are collected in Table S1. The ORTEP drawings of the molecular structures, selected bond lengths, and inter-ring twist dihedral angles are summarized in Table 1. All of these molecules exhibit consistently large arene−arene dihedral twist angles (80−89°). The (ring)C−C(ring) distances in these molecules are slightly longer than in typical biaryls (~1.487 Å)[38] and close to that in bimesityl (1.505(2) Å),[39] doubtless a result of the pronounced steric hindrance about this region of the molecules.
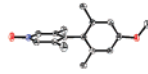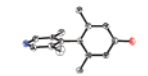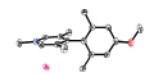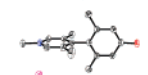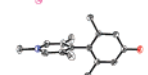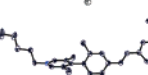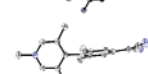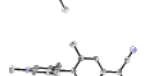
The (ring)C−C(ring) and (ring)C−O distances in the two zwitterionic **TM** chromophores **TM-1** and **TM-2** are only modestly shorter than in those of the corresponding neutral (**3**, **6**) and positively charged (**5**, **7**) species (Table 1), probably a result of the very small contribution of quinoidal limiting forms (Chart 1) to the ground state due to the twist-induced intra-

(37) Abbotto, A.; Bradamante, S.; Facchetti, A.; Pagani, G. A. *J. Org. Chem.* **1997**, *62*, 5755.

(38) Database of average bond lengths in organic compounds: Allen, F. H.; Kennard, O.; Watson, D. G.; Brammer, L.; Orpen, A. G.; Taylor, R. *J. Chem. Soc., Perkin Trans. 2* **1987**, S1.

(39) Fröhlich, R.; Musso, H. *Chem. Ber.* **1985**, *118*, 4649.

Table 1. ORTEP Drawings of the Molecular Structure and Selected Metrical Parameters for Twisted π-Electron System Chromophores and Several Synthetic Intermediates

twisted molecule species	ORTEP drawing of the molecular structure [a]	(ring)C•C(ring) (Å)	(ring)C•O (Å)	(ring)C•C(CN)$_2$ (Å)	twist angle (°)[b]
3		1.5006(18)	1.3767(16)	-	84.2
6		1.4932(18)	1.3579(17)	-	85.7
5		1.496(3)	1.372(3)	-	87.9
7		1.496(3)	1.364(3)	-	86.1
TM-1		1.489(2)	1.312(2)	-	86.9
TM-2		1.490(5)	1.305(4)	-	87.5
TMC-1[c]		1.501(2) 1.492(2)	-	1.456(2) 1.455(2)	79.9 85.6
TMC-2		1.488(5)	-	1.463(5)	89.6

[a] Drawn with 50% probability ellipsoids. Hydrogen atoms and solvent molecules are omitted for clarity. The iodide counterions are included in the drawings of **5** and **7**. [b] Average of four dihedral angles in the respective crystal structures. [c] There are two independent molecules in the **TMC-1** unit cell.

molecular charge transfer (see more below). Thus, there is a pronounced reduction in inter-ring π conjugation, and a dominant zwitterionic ground state prevails in all of the **TM** chromophores, evidenced by the departure from quinoidal structures where typically (ring)C=C(ring) $\approx$ 1.349 Å and C=O $\approx$ 1.222 Å.[38]

Similar structural characteristics are revealed in the **TMC** chromophores. The observed (ring)C—C(ring) distances imply strong reduction in inter-ring π conjugation. The phenylenedi-cyanomethanide fragments display a markedly different bond length pattern than in typical TCNQs.[38,40] The (NC)$_2$C-bound phenylene rings exhibit significantly less quinoidal character, and the (dicyanomethanide)C—C(aryl) distances lack typical TCNQ C=C(CN)$_2$ exocyclic character ($\sim$1.392 Å).[38] This indicates substantial negative charge localization within the —C(CN)$_2$ group, also evident from the observed C—CN bond shortening (1.397(2)—1.412(2) Å in **TMC-1** and 1.402(5)—1.402(6) Å in **TMC-2** vs 1.427 Å in typical TCNQs[38]), and C≡N bond elongation (1.152(2)—1.158(2) Å in **TMC-1**, 1.160(5)—1.165(6) Å in **TMC-2**, vs 1.144 Å in typical TCNQs[38]), a result of charge resonant stabilization via the two CN groups. Finally, there is significant pyridinium aromatic character in the **TMC** chromophores with metrical parameters paralleling *N*-methyl-*p*-phenylpyridinium salts[41] rather than

cyclopentadienylidene-1,4-dihydropyridines.[42] Taken together, the solid-state metrical parameters confirm a highly charge-separated zwitterionic **TMC** ground state (cf., Chart 2).

The solid-state packing diagrams of chromophores **TM-1**, **TM-2**, **TMC-1**, and **TMC-2** are shown in Figure 1. All of the present zwitterions crystallize in antiparallel pairs, doubtless a result of electrostatic interactions[43] involving their large dipole moments.[44] The **TM-1** molecules exist in the crystal as a complex with NaI units where two molecules are linked head-to-head by Na$^+$ ions, a result of the strong phenoxide affinity for Na$^+$ (Figure 1A). A centrosymmetric dimer of two dimeric complexes is linked between two neighboring zwitterions from each complex, arrayed in an antiparallel fashion with an intermolecular distance of 6.475 Å between the aromatic backbones. This distance is considerably larger than the sums of van der Waals radii between planar cofacial π-electron systems ($\sim$ 3.50 Å)[43] and is likely the result of the difficulty in closely face-to-face packing the aromatic rings in these sterically encumbered twisted π-electron molecules. The dimers are arranged within the (101) plane in a herringbone-like packing with an angle of 30° between the backbones of adjacent dimers. **TM-2** molecules are arrayed along the *a* direction in loosely interacting antiparallel pairs. These dimers have a larger

(40) Cole, J. C.; Cole, J. M.; Cross, G. H.; Farsari, M. J.; Howard, A. K.; Szablewski, M. *Acta Crystallogr.* **1997**, *B53*, 812.
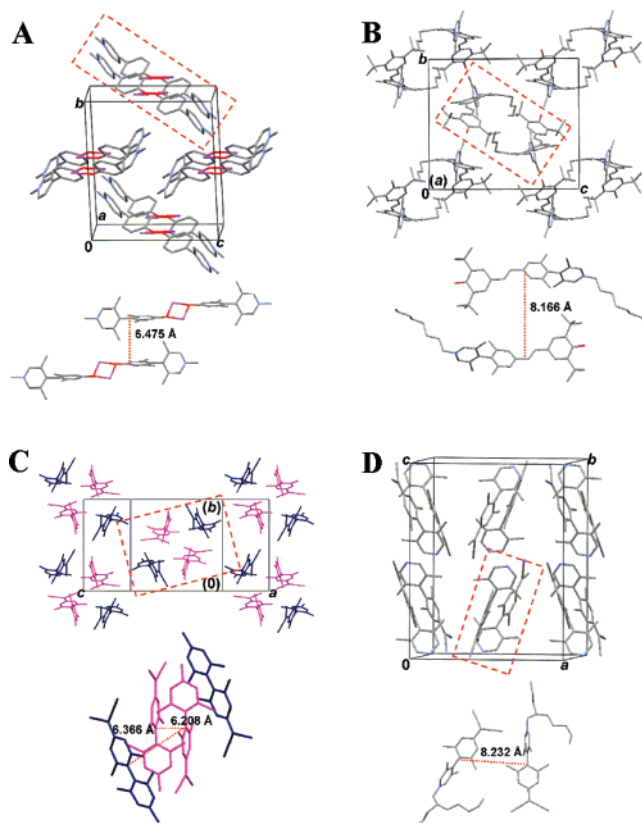(41) Das, A.; Jeffery, J. C.; Maher, J. P.; McCleverty, J. A.; Schatz, E.; Ward, M. D.; Wollermann, G. *Inorg. Chem.* **1993**, *32*, 2145.
(42) Ammon, H. L.; Wheeler, G. L. *J. Am. Chem. Soc.* **1975**, *97*, 2326.
(43) Würthner, F.; Yao, S.; Debaerdemaeker, T.; Wortmann, R. *J. Am. Chem. Soc.* **2002**, *124*, 9431.
(44) DFT-derived ground-state dipole moments are 20.0, 37.3, 27.0, and 50.6 D for **TM-1**, **TM-2**, **TMC-2**, and **TMC-3**, respectively.

Figure 1. Crystal packing diagrams of chromophores **TM-1** (A), **TM-2** (B), **TMC-1** (C), and **TMC-2** (D). A single dimeric or tetrameric unit is indicated by the dashed lines and shown at the bottom. The two independent molecules in the **TMC-1** asymmetric unit are colored by symmetry equivalence. Solvent molecules (A−C), tetra-*o*-methyl substituents (A, top), and *N*-alkyl chains (D, top) are removed for clarity.

separation than that in the aforementioned **TM-1** dimer, 8.166 Å, clearly a result of steric hindrance from the bulky *tert*-butyl groups and *N*-alkyl chains. The structures of **TMC-1** and **TMC-2** exhibit similar but more complex packing features. A tetramer-like unit is found in the **TMC-1** unit cell (Figure 1C) consisting of two independent molecules with a distance of 6.208 Å between two neighboring molecules oriented in an antiparallel fashion and an average distance of 6.366 Å between two skew-packed neighbors. The formation of tetramers is consistent with strong dipolar interactions between **TMC** molecules, doubtless a consequence of their large dipole moments.[44] In the case of **TMC-2**, which possesses a bulky *N*-alkyl chain at the pyridinium fragment, the two molecules in the dimeric unit are forced apart to accommodate the bulky chain with a larger average intermolecular distance of 8.232 Å (Figure 1D). This asymmetric dimer is related to the neighboring dimer via an inversion center to form the centrosymmetric unit cell.

Twist Angle Measurement in Solution by NOE. Nonlinear least-squares fitting of experimental σ_{IS} values (see Experimental Section for details) as a function of temperature according to eq 5 (Figure 2A) yields r_{IS}, E_R, and τ^0 parameters. The results are summarized for **TMC-2** in Table 2. The r_{43} distance is independent of the dihedral twist angle and can test the validity of this methodology. The obtained value from the NOE measurements ($r_{43} = 2.7 \pm 0.1$ Å) is in excellent agreement with that calculated from the solid-state structure under r^{-6} averaging (2.68 and 2.83 Å for the two limiting static conforma-
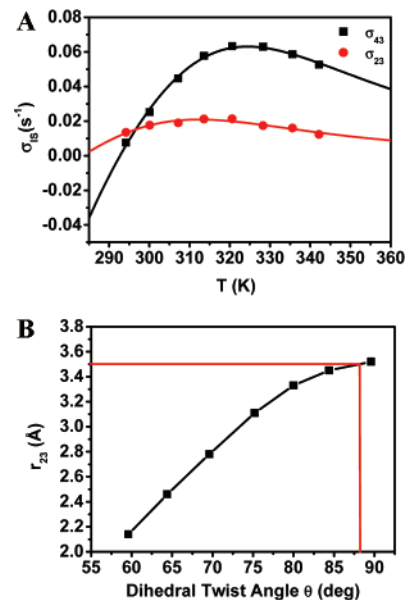
Figure 2. (A) Nonlinear regression analysis of the cross-relaxation rate constant σ_{IS} for **TMC-2** measured from NOE NMR in dry DMSO-d_6 as a function of temperature according to eq 5. The solid lines are the best fit to the data. (B) Computed distance r_{23} for **TMC-2** as a function of dihedral twist angle. The cross point indicates the NOE-derived distance r_{23} and the corresponding twist angle.

Table 2. Internuclear Distance r_{IS} (Å),[a] Activation Energy for Rotational Reorientation E_R (kJ/mol), τ^0 (10^{-15} s) Values Estimated from the Best Nonlinear Least-Squares Fit of NOE Data for **TMC-2**, and the Corresponding Correlation Time τ_C (10^{-15} s) at 300.1 K

	r_{IS}	E_R	τ^0	τ_C
H4−H3	2.7 ± 0.1	26.7 ± 0.8	7.5 ± 2.3	343
H2−H3	3.5 ± 0.2^a	27.4 ± 2.6	3.9 ± 4.1	232

[a] r_{23} average distance obtained from the nonlinear least-squares fit has been incremented by 10% to account for the overestimation of short distances due to conformational averaging.[20]

tions of the methyl group). The dependence of the distance r_{23} on the dihedral angle (θ) was then computed in the 60−90° range using the solid-state structure as described in the Experimental Section, and the relationship is plotted in Figure 2B. From the plot, an average dihedral angle θ of 88° ± 10°, corresponding to the derived r_{23} of 3.5 ± 0.2 Å (Table 2), can be estimated in solution, in excellent agreement with the solid-state structures (Table 1).

Optical Spectroscopy. All the tictoid chromophores exhibit intense optical absorption in the UV−vis region with extinction coefficients as large as 38 400 M^{-1} cm^{-1}. Optical maxima λ_{max}, extinction coefficients ϵ and the lowest energy optical gaps E_g (estimated from the onset of the absorption maxima at the low-energy edges) are collected in Table 3. **TM** chromophore optical absorption spectra in methanol are shown in Figure 3A. The **TM-1** optical spectrum consists of two maxima at 269 (ϵ = 6900 M^{-1} cm^{-1}) and 400 nm (ϵ = 790 M^{-1} cm^{-1}), assignable to phenyl subfragment intra-ring excitations and inter-subfragment charge-transfer (CT) excitation, respectively.[15] Pyridinium intra-subfragment excitation is expected to be at higher energy[15] and overlap with the solvent cutoff. Such a modest extinction coefficient for the CT band indicates a pronounced reduction in inter-ring π conjugation due to the twist. The **TM-2** spectrum

Table 3. Optical Absorption (λ_{max}, nm, and Extinction Coefficient ϵ, M^{-1} cm^{-1}) Data, Optical Gap E_g (eV), Redox Potentials E vs SCE (V), Estimated Ground-State Dipole Moments μ_g (D), and the Maximum EFISH-Derived $\mu\beta$ Values (10^{-48} esu) for **TM** and **TMC** Chromophores

| compound | λ_{max} (ϵ) | | | $E_g{}^d$ | E^e | | $\mu_g{}^f$ | $\mu\beta$ | |
	MeOH	CH_3CN	CH_2Cl_2	CH_3CN	E_{ox}	E_{red}		CH_2Cl_2	DMF
TM-1	269^a (6900)	304^a				-1.54			
				2.04	0.30		20.0		
TM-2	400^b (790) 326^a (20700)	474^b				-1.65			
		448^a	462^a	2.32	1.25	-1.64	37.3	-315000	-49000
TMC-1	495^b (2010) 296^a	304^a	314^a						
				2.24			27.0		
TMC-2	440^b 297^a	462^b 304^a	556^b 314^a (27200)						
				2.16	0.39	-1.56	27.0	-24000	-5620
TMC-3	451^b 397^a	472^b 416^a	569^b (1840) 433^a (38400) 540^c (2090)	2.61	0.20	-1.50	50.6	-488000	-84000

^{a} Assigned to intra-subfragment excitation. Another high-energy subfragment excitation overlaps with the solvent and is not tabulated here. ^{b} Assigned to low-energy inter-subfragment charge-transfer (CT) excitation. ^{c} Deconvoluted from the subfragment excitation band and assigned to inter-subfragment CT. ^{d} Estimated from the onset of the absorption maximum at the low-energy edge. ^{e} Referred to ferrocene internal reference $E_{1/2} = 0.43V$ vs SCE in MeCN. ^{f} DFT-derived ground-state dipole moment.
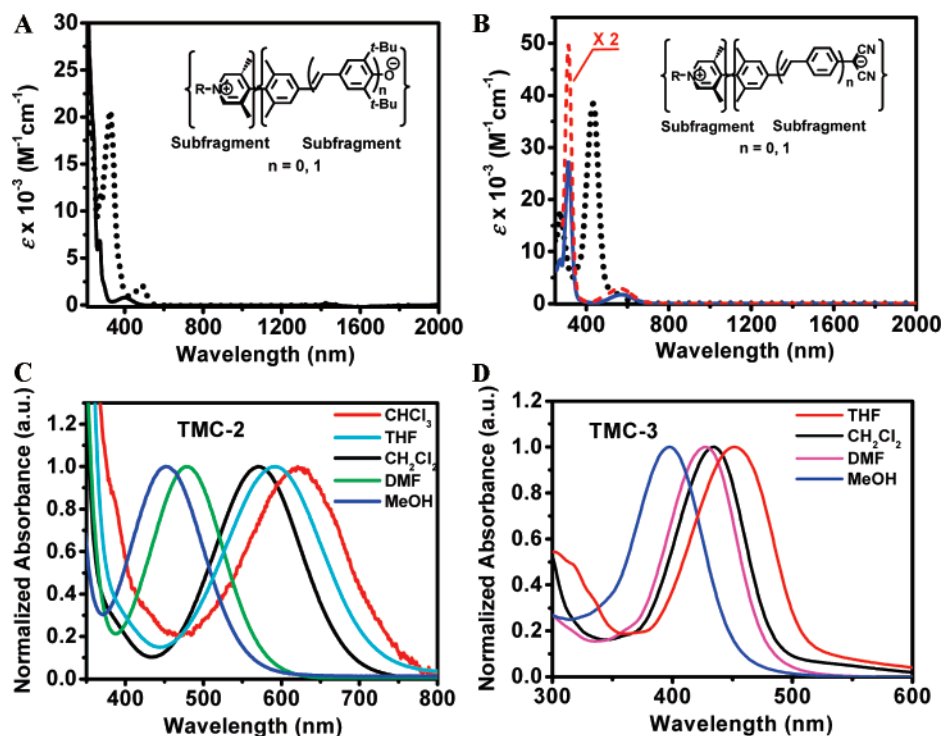
Figure 3. (A) Optical absorption spectra of **TM** chromophores in methanol solution: solid line, **TM-1**; dotted line, **TM-2**. (B) Optical absorption spectra of **TMC** chromophores in CH_2Cl_2 solution: dashed line, **TMC-1** (enlarged for clarity); solid line, **TMC-2**; dotted line, **TMC-3**. (C) Optical absorption spectra of **TMC-2** in different solvents. Only interfragment CTs band are shown here. (D) Optical absorption spectra of **TMC-3** in solvents of varying polarity. Inter- and intrafragment excitation bands are overlapped.

also features an intense band at 326 nm ($\epsilon = 20\,700$ M^{-1} cm^{-1}), assigned to stilbenyl subfragment excitation and a relatively weak CT band at 495 nm ($\epsilon = 2010$ M^{-1} cm^{-1}) with a shoulder at short wavelength. All of the **TM** chromophores have limited solubilities in moderate- and low-polarity solvents, precluding a full comparative optical spectroscopic study as a function of solvent.

The **TMC** chromophore optical properties were studied in a range of solvents having varying polarity. Their spectra in CH_2-Cl_2 are shown in Figure 3B. It can be seen that **TMC-1** and **TMC-2** exhibit similar spectra with two fairly short wavelength maxima, tentatively assigned to pyridinium and phenyl sub-

fragment high-energy intra-ring excitations, and one low-energy inter-subfragment charge-transfer (CT) excitation (Figure 3B).[15] The CT band has a smaller oscillator strength ($\lambda_{max} = 569$ nm, $\epsilon = 1840$ M^{-1} cm^{-1} for **TMC-2** in CH_2Cl_2) than the intra-subfragment excitation band ($\lambda_{max} = 314$ nm, $\epsilon = 27\,200$ M^{-1} cm^{-1} for **TMC-2** in CH_2Cl_2). The principal difference between the **TMC-1** and **TMC-2** spectra is that the **TMC-1** CT band is slightly blue shifted vs that of **TMC-2**, suggesting that any aggregation (reasonable considering the large dipole moments[44]) is greater for methyl-functionalized **TMC-1** than for bulky alkyl-functionalized **TMC-2**. Such CT band blue shifts due to antiparallel centrosymmetric dimer formation have also been

reported in merocyanine dye aggregation studies.[43] Figure 3C shows **TMC-2** optical absorption spectra in solvents of different polarity. It can be seen that the **TMC-2** CT bands exhibit strong *negative* solvatochromic effects—large blue shifts with increasing solvent polarity (the spectra were recorded in the concentration range where the aggregation is not significant). The **TMC-2** solvatochromic shift from CHCl$_3$ to MeOH is ∼153 nm toward shorter wavelength, comparable to the largest solvatochromic effects reported in heavily studied betaine[45] and merocyanine derivatives.[4d,37,46] Within the conventional interpretation of solvatochromic interactions,[47] the negative solvatochromism indicates that the magnitude of the dipole moment in the excited electronic state is significantly smaller than in the ground state. Although other factors can affect the sign of solvatochromism (e.g., aggregation or different solvent polarizabilities),[48] within the reasonable hypothesis that the various solvents here do not drastically affect the electronic nature of the ground and excited states, the negative solvatochromism indicates that the **TMC** ground state is best approximated by the zwitterionic limit formula. The intra-subfragment excitation bands exhibit similar but weaker negative solvatochromism. The **TMC-3** optical spectrum (Figure 3B) features an intense band centered at ∼433 nm in CH$_2$Cl$_2$ (ϵ = 38 400 L mol^{-1} cm^{-1}) assigned to predominant stilbenyl subfragment excitation, overlapping a relatively weak CT band centered at 540 nm (ϵ = 2090 M^{-1} cm^{-1}). Both subfragment and CT bands (a CT band of 578 nm can be deconvoluted from the subfragment excitation band in THF) exhibit negative solvatochromism (Figure 3D).

Solid-state optical studies were also performed on films of **TMC-2** and **TMC-3** prepared by spin-coating chromophore cyclopentanone solutions onto fused quartz slides followed by drying in a vacuum oven. The optical spectra of these films exhibit close correspondences to those acquired in DMF solution (Figure 4). Taking into account the negative solvatochromic shift of the CT excitations and aggregation effects (vide supra), the spectral patterns exhibit no significant differences between the solid state and solution phase.

Electrochemistry. Cyclic voltammetry (CV) was carried out under N$_2$ in a 0.1 M Bu$_4$NPF$_6$ solution in anhydrous MeCN with scanning rates between 60 and 150 mV/s. Voltammograms of ∼10^{-3} M CH$_3$CN solutions of **TM-1**, **TM-2**, **TMC-2**, and **TMC-3** exhibit one chemically irreversible oxidation wave and one irreversible reduction wave (two in **TM-1**), which can be attributed to the redox chemistry of the phenoxide/phenyldicynomethanide donor and the pyridinium acceptor moieties. Data are summarized in Table 3. All the chromophores exhibit comparable reduction potentials. The surprisingly high oxidation potentials of **TM-2** can be attributed to weak solvation of its cation radical, possibly due to the steric effects of the two *ortho* tert-butyl substituents at the phenoxide portion. HOMO−LUMO (electrochemical) gaps can be estimated from the oxidation and reduction potentials. We are aware that a precise E_{gap} determination requires knowledge of the standard potentials. However, from the present oxidative/reductive data, we estimate HOMO−
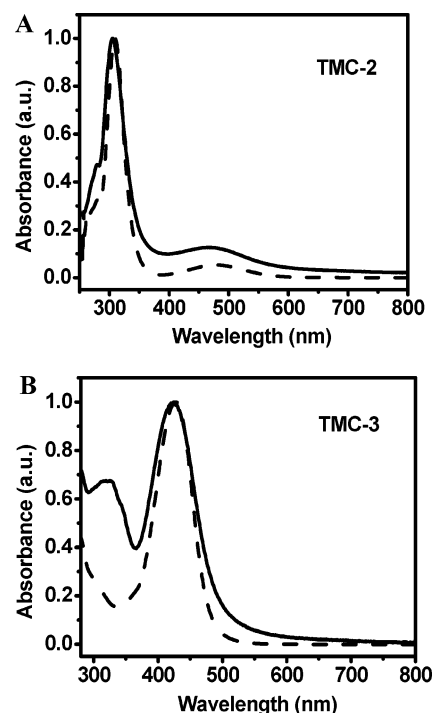
Figure 4. Optical absorption spectra of **TMC-2** (A) and **TMC-3** (B) in the solid state (solid line) vs those in DMF solution (dashed line).

LUMO gaps of ∼1.84 and ∼1.95 eV for **TM-1** and **TMC-2**, respectively, in good agreement with the optical gaps (Table 3). In the case of **TM-2** and **TMC-3**, there are considerable discrepancies between the electrochemical gaps and the optical gaps (Table 3), perhaps because the HOMO−LUMO optical transitions are mixed with other transitions.

Infrared Vibrational Spectroscopy. The IR spectra of chromophores **TM-1**, **TM-2**, **TMC-2**, and **TMC-3** are shown in Figure 5. Both **TM-1** and **TM-2** exhibit several sharp, intense infrared transitions in the 1000−1800 cm^{-1} region (Figure 5A), which correspond to principally aromatic ring stretching modes. The features at 1585 cm^{-1} in **TM-1** and 1578 cm^{-1} in **TM-2** correspond to the aromatic stretching modes typical of phenoxide rings.[49] The C=O stretching mode ν(C=O), which is usually the strongest band at 1640−1660 cm^{-1} in typical benzoquinone structures,[50] is very weak or nonexistent in **TM-1** (∼1640 cm^{-1}) and **TM-2** (∼1636 cm^{-1}), arguing for only very small quinoidal limit contribution to the **TM** ground state.

In the **TMC** infrared spectra (Figure 5B and 5C), the CN stretching vibration, ν(C≡N), is observed for both **TMC-2** and **TMC-3** as the most intense band at around 2164 cm^{-1} with a low-energy side component (2126 cm^{-1} in **TMC-2** and 2118 in **TMC-3**). This two-peak feature is also observed in some dianionic TCNQs and zwitterionic dicynomethylene derivatives[4b,51] with the more intense band assigned to an in-phase ν(C≡N) normal mode and the second to the related out-of-phase motion.[4b, 51] In contrast, compounds **15** and **19**, the neutral precursors to **TMC-2** and **TMC-3**, respectively, exhibit only a very weak transition at 2257 cm^{-1}. The ν(C≡N) energy is known to be highly sensitive to the electron density localization

(45) Reichardt, C. *Chem. Rev.* **1994**, *94*, 2319.
(46) Citterio, D.; Kawada, T.; Yagi, J.; Ishigaki, T.; Hisamoto, H.; Sasaki, S.; Suzuki, K. *Anal. Chim. Acta* **2003**, *482*, 19.
(47) *Solvents and Solvent Effects in Organic Chemistry 2*; Reichardt, C., Ed.; VCH: Weinheim, 1990.
(48) Chen, C.-T.; Marder, S. R. *Adv. Mater.* **1995**, *7*, 1030.
(49) Kotorlenko, L. A.; Aleksandrova, V. S.; Yankovich, V. N. *J. Mol. Struct.* **1984**, *115*, 501.

(50) Yates, P.; Ardao, M. I.; Fieser, L. F. *J. Am. Chem. Soc.* **1950**, *78*, 650.
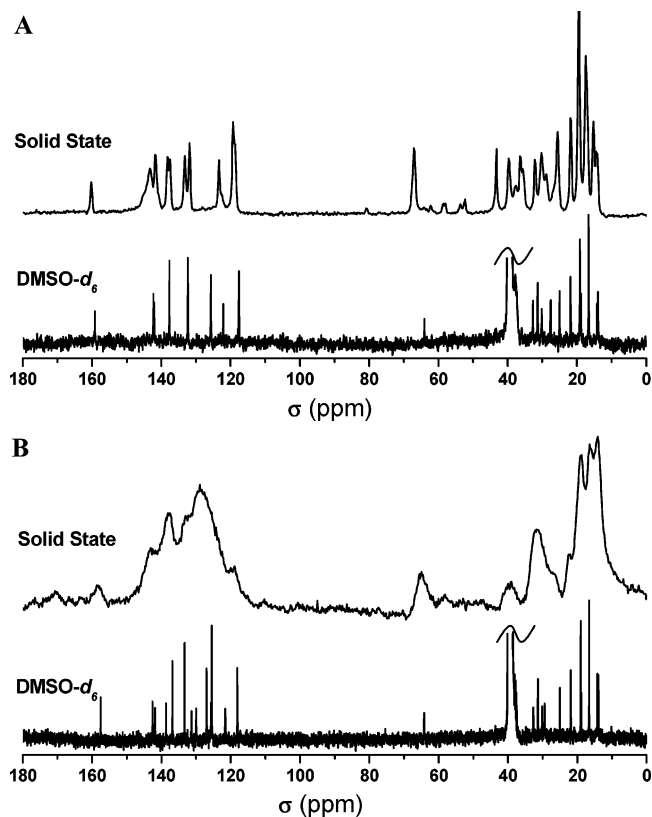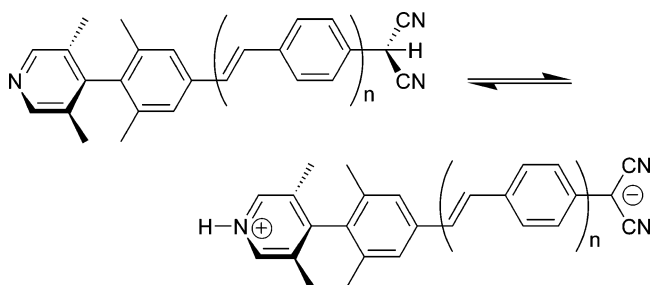(51) Casado, J.; Pappenfus, T. M.; Mann, K. R.; Milián, B.; Ortí, E.; Viruela, P. M.; Ruiz Delgado, M. C.; Hernández, V.; López Navarrete, J. T. *J. Mol. Struct.* **2003**, *651−653*, 665.
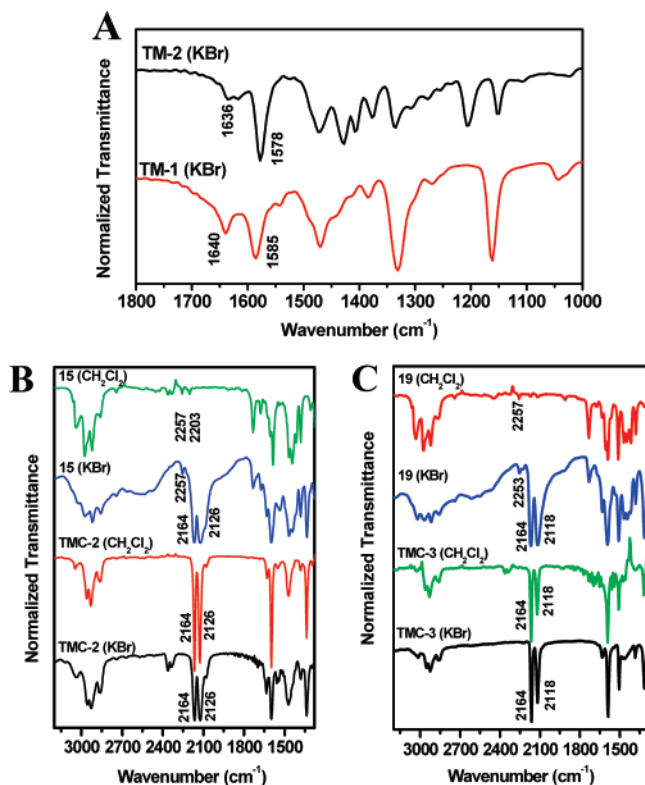
Figure 5. (A) IR spectra of chromophores **TM-1** and **TM-2** as KBr pellets. (B) IR spectra of **TMC-2** and its neutral precursor **15** in a KBr pellet and CH₂Cl₂ solution. (C) IR spectra of **TMC-3** and its neutral precursor **19** in a KBr pellet and CH₂Cl₂ solution.

onto the C≡N fragment,[52] e.g., converting phenylmalononitrile into the corresponding carbanion is accompanied by a strong decrease of the CN stretching frequency (for phenylmalononitrile ν(C≡N) = 2254 cm^{-1} versus ν(C≡N) = 2163, 2117 cm^{-1} in the carbanion), dramatic increases in the corresponding integrated intensities (~136-fold), and strong enhancement of the oscillator−oscillator ν(C≡N) vibrational coupling (ν(C≡N) splitting = 46 cm^{-1}).[52a] Thus, the electron density localized on the dicyanomethanide fragments of **TMC-2** and **TMC-3** is qualitatively similar to that of the phenylmalononitrile carbanion,[52a] where the dicyanomethanide unit supports nearly one negative charge. Furthermore, note that both the **TMC-2** and **TMC-3** IR spectra recorded in the solid state (KBr pellet) and solution (CH₂Cl₂) are virtually identical, indicating very similar electron density distributions, hence similar molecular structural characteristics, in the solid state and solution. One interesting observation is that neutral precursors **15** and **19** exhibit similar spectral features in the solid state (KBr pellet) which are very similar to those of the corresponding zwitterions (Figure 5B and 5C), implying a possible proton transfer between the strong acidic dicyanomethylene group and pyridine group. It was not


possible to obtain diffraction-quality crystals of precursors **15** and **19**.

Solid-State vs Solution NMR Spectroscopy. Solid-state CPMAS ¹³C NMR and solution-phase ¹³C NMR spectra of chromophores **TMC-2** and **TMC-3** are compared in Figure 6. Comparison of solid-state NMR spectra with those in solution provides additional insights into chromophore molecular structure and electronic charge distribution in the solid state vs solution since any significant change in twist angle should drastically shift the distribution between zwitterionic and quinoidal electronic structures and hence the chemical shifts of the nuclei proximate to the π-electron core. A change of one electron in π-electron density for a π-conjugated system is expected to result in a total change of ~160 ppm in carbon atom chemical shift.[53] As can be seen in the NMR spectra, the **TMC-2** resonance positions (Figure 6A) are virtually identical in the solid state and DMSO-d_6. The signals adjacent to the positively charged pyridinium center in the solid-state NMR spectra, δ (N-CH₂, 67.2 ppm) and δ (pyr, 160.3 ppm), are displaced only 3.2 and 1.1 ppm upfield, respectively. Furthermore, **TMC-3** ¹³C NMR spectra in the solid state and DMSO-d_6 are nearly identical (Figure 6B) with only a minor change of 0.3 ppm in δ (N-CH₂, 64.5 ppm) and 0.7 ppm in δ (pyr, 158.2 ppm). These results exclude any significant changes in molecular twist angles on going from the condensed state to the solution phase, consistent with the observations in the optical and IR spectra discussed above.

Figure 6. (A) ¹³C NMR spectra of chromophore **TMC-2** in the solid state (top) and DMSO-d_6 solution (bottom). (B) ¹³C NMR spectra of chromophore **TMC-3** in the solid state (top) and DMSO-d_6 solution (bottom).

(52) (a) Binev, Y. I.; Georgieva, M. K.; Novkova, S. I. *Spectrochim. Acta.* **2003**, *59A*, 3041. (b) Taylor, R.; Kennard, O. *J. Am. Chem. Soc.* **1982**, *104*, 5063.
(53) Bradamante, S.; Pagani, G. A. *J. Chem. Soc., Perkin Trans. 2* **1986**, 1035.
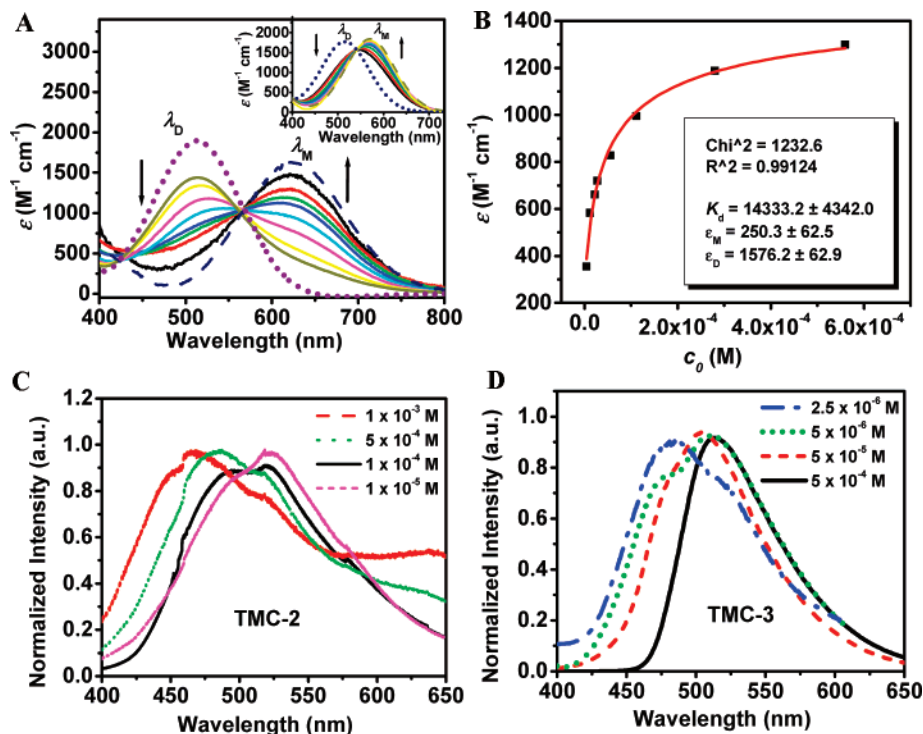
Figure 7. (A) Concentration-dependent **TMC-2** optical spectra in CHCl$_3$ solution. Arrows indicate changes in CT bands upon dilution from 5.5×10^{-4} to 4.5×10^{-6} M. (Inset) Concentration-dependent **TMC-2** optical spectra in CH$_2$Cl$_2$ solution (3.0×10^{-3}–2.0×10^{-5} M). The monomer (dashed line) and dimer (dotted line) spectra were derived from data at two different concentrations and K_{dimerize} according to eq 12. (B) A typical nonlinear regression analysis of the **TMC-2** apparent extinction coefficient ϵ as a function of concentration c_0 at 490 nm in CHCl$_3$ solution according to eq 12. The solid line is the best fit to the data. (C) Variable-concentration fluorescence spectra (λ_{ex} = 350 nm) of **TMC-2** in CH$_2$Cl$_2$. (D) Variable-concentration fluorescence spectra (λ_{ex} = 300–350 nm) of **TMC-3** in CH$_2$Cl$_2$. Intensities are normalized for clarity.

Studies of TMC Chromophore Aggregation in Solution by Optical Absorption and Fluorescence Spectroscopies. The aggregation state of chromophore **TMC-2** in solution was studied by variable-concentration optical spectroscopic methods.[43] Significant **TMC-2** spectral changes in moderately polar CHCl$_3$ (ϵ_r = 4.81) solutions can be observed upon variation of the concentration over the range 5.5×10^{-4}–4.5×10^{-6} M (Figure 7A). The spectra at highest dilution can be ascribed to the monomeric chromophore with a CT band centered around 621 nm. Upon increasing the concentration, the spectra exhibit diminution of this CT band and concomitant appearance/growth of a new transition at shorter wavelength, revealing the onset of aggregation. A well-defined isosbestic point clearly is consistent with equilibrium between monomer (M) and dimer (D). Pragmatically employing the simplest dimerization model for the moment (2M ⇌ D), the dimerization constant K_d can be defined as

$$K_d = \frac{c_D}{c_M^2} = \frac{1-\alpha}{2\alpha^2 c_0} \tag{10}$$

where c_D and c_M are the equilibrium concentrations of dimer and monomer, respectively, c_0 is the initial concentration, and α is the fraction of the monomer in solution, defined as $\alpha = c_M/c_0$. The apparent extinction coefficient ϵ can then be expressed as

$$\epsilon = \epsilon_M \alpha + \epsilon_D (1-\alpha) \tag{11}$$

where ϵ_M and ϵ_D are extinction coefficients of monomer and

dimer, respectively. Combining eqs 10 and 11 yields an expression for the apparent extinction coefficient ϵ as

$$\epsilon = \frac{\sqrt{8K_d c_0 + 1} - 1}{4K_d c_0} (\epsilon_M - \epsilon_D) + \epsilon_D \tag{12}$$

Nonlinear regression analysis (Figure 7B) of ϵ as a function of solution concentration at a specific wavelength based on eq 12 yields K_d = 13 300 ± 1420 M^{-1} (average of the nonlinear regression analysis data at six different wavelengths), and the related Gibbs dimerization energy ΔG°_d = −23.5 ± 0.3 kJ mol^{-1} can be derived from eq 13

$$\Delta G^\circ_d = -RT \ln K_d \tag{13}$$

The respective monomer and dimer spectra can be then calculated from the derived K_d and the absorption data at two different concentrations according to eq 12 (Figure 7A). Concentration-dependent **TMC-2** optical absorption studies in more polar CH$_2$Cl$_2$ (Figure 7A, inset) indicate similar aggregation effects but at higher concentration ranges (10^{-4}–10^{-3} M). Nonlinear regression analysis yields smaller K_d and ΔG^0_d values of 246 ± 30 M^{-1} and −13.6 ± 0.3 kJ mol^{-1}, respectively.

The **TMC-2** aggregation in CH$_2$Cl$_2$ is also evidenced from variable-concentration fluorescence spectra despite the low emission intensity. Significant **TMC-2** spectral changes can be observed upon variation of the concentration over the range 1×10^{-3}–1×10^{-5} M (Figure 7C) with a transition from λ_{em} = 462 to 522 nm, in good agreement with the concentration variation range in optical absorption spectral data. **TMC-3**
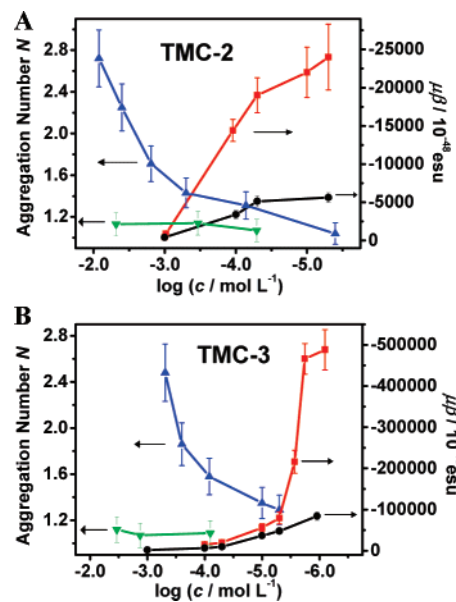
Table 4. Diffusion Coefficient (D_t, 10^{-10} m^2 s^{-1}), Hydrodynamic Radius (r_H, Å), Hydrodynamic Volume (V_H, Å^3), and Aggregation Number ($N = V_H/V_{vdW}{}^a$) for **TMC-2** and **TMC-3** as a Function of Concentration c

entry	solvent	c (mM)	D_t	r_H	V_H	N
			TMC-2			
1	CD$_2$Cl$_2$	0.004	10.0(6)	4.60	408	1.0(4)
2	CD$_2$Cl$_2$	0.07	9.3(2)	4.96	512	1.3(1)
3	CD$_2$Cl$_2$	0.5	9.0(5)	5.11	558	1.4(3)
4	CD$_2$Cl$_2$	1.6	8.5(2)	5.43	670	1.7(1)
5	CD$_2$Cl$_2$	4.0	7.7(7)	5.95	881	2.2(5)
6	CD$_2$Cl$_2$	8.4[b]	7.3(0)	6.33	1064	2.7(3)
7	DMSO-d_6	0.05	1.9(9)	4.64	417	1.1(3)
8	DMSO-d_6	0.34	1.9(4)	4.74	448	1.1(4)
9	DMSO-d_6	4.83	1.9(5)	4.72	440	1.0(7)
			TMC-3			
10	CD$_2$Cl$_2$	0.005	7.9(7)	5.32	630	1.2(9)
11	CD$_2$Cl$_2$	0.01	7.8(7)	5.39	654	1.3(5)
12	CD$_2$Cl$_2$	0.083	7.4(6)	5.68	769	1.5(8)
13	CD$_2$Cl$_2$	0.25	7.0(7)	5.99	903	1.8(6)
14	CD$_2$Cl$_2$	0.49[b]	6.4(2)	6.60	1205	2.4(8)
15	DMSO-d_6	0.08	1.6(8)	5.02	529	1.1(2)
16	DMSO-d_6	1.34	1.6(9)	4.99	522	1.0(7)
17	DMSO-d_6	3.4	1.6(6)	5.07	547	1.0(9)

[a] van der Waals volumes: **TMC-2**, 389 Å^3 (from X-ray data); **TMC-3**, 486 Å,^{3} computed from X-ray data of **TMC-2** adding the volume of a styryl moiety (97 Å^3)]. [b] Saturated solution.

aggregation is more difficult to observe in optical absorption spectroscopy due to overlapped CT transitions (Figure 3B). Alternatively, variable-concentration **TMC-3** fluorescence spectra in CH$_2$Cl$_2$ (Figure 7D) reveal a clear transition from dimer (515 nm) to monomer (485 nm) emission upon dilution in the range of 5×10^{-4}–2.5×10^{-6} M. Although quantitative aggregation information is difficult to estimate in fluorescence spectra due to the quenching of fluorescence in aggregates, these results provide further evidence of **TMC** aggregation.

PGSE NMR Measurements on TMC Chromophores. PGSE (pulsed field gradient spin–echo) NMR techniques[54] represent an incisive tool to quantify molecular dimensions in solution and, consequently, levels of aggregation.[26] Experimentally determined translational self-diffusion coefficients (D_t), hydrodynamic radii (r_H), volumes (V_H), and the ratio between V_H and the van der Waals volume (V_{vdW}) afford aggregation numbers N ($N = V_H/V_{vdW}$) readily indicating aggregation levels in solution ($N = 1.0, 1.5,$ or 2.0 indicates 100% monomer, 50% monomer + 50% dimer, or 100% of dimer, respectively).[26a] Table 4 summarizes the results of the PGSE measurements carried out on chromophores **TMC-2** and **TMC-3** in both CD$_2$-Cl$_2$ and DMSO-d_6 over a broad range of concentrations. The variation in the aggregation number N as a function of the concentration is shown in Figure 8. The trends in N vs concentration (Table 4, Figure 8) clearly show that monomer predominates in very polar DMSO-d_6 ($\epsilon_r{}^{25} = 46.45$) for both **TMC-2** and **TMC-3** over the entire concentration range (Table 4, entries 7–9 and 15–17). In CD$_2$Cl$_2$ ($\epsilon_r{}^{25} = 8.93$), **TMC-2** is exclusively monomeric only at the lowest concentrations examined (4×10^{-6} M, Table 4, entry 1) while dimers (Table 4, entries 4–5) and even somewhat larger aggregates ($N = 2.7$, Table 4, entry 6) are present at the highest concentrations (Figure 8). **TMC-3** exhibits a greater tendency for aggregation and is not exclusively monomeric even at 5×10^{-6} M (Table 4, entry

(54) (a) Johnson, C. S., Jr. *Prog. Nucl. Magn. Reson. Spectrosc.* **1999**, *34*, 203.
    (b) Stilbs, P. *Prog. Nucl. Magn. Reson. Spectrosc.* **1987**, *19*, 1.

Figure 8. Comparative PGSE NMR-derived aggregation number (N, left scale) data and EFISH-derived $\mu\beta$ data (right scale) as a function of concentration for twisted chromophores **TMC-2** (A) and **TMC-3** (B). PGSE NMR data are obtained from CD$_2$Cl$_2$ (▲) and DMSO-d_6 (▼) solutions. EFISH measurements are performed in CH$_2$Cl$_2$ (■) and DMF (●) solutions. Lines are drawn as guides to the eye. c = concentration.

10). For **TMC-3**, aggregates somewhat larger than dimers are determined to be present at the highest concentrations ($N = 2.4$, Table 4, entry 14).

**Hyperpolarizability Measured by EFISH Spectroscopy.** EFISH-derived $\mu\beta$ values for chromophores **TM-2**, **TMC-2**, and **TMC-3** in CH$_2$Cl$_2$ and DMF are summarized in Table S3. The variation of the $\mu\beta$ values for **TMC-2** and **TMC-3** as a function of the concentration is shown in Figure 8 in comparison with PGSE-derived aggregation numbers. In less polar CH$_2$Cl$_2$ the $\mu\beta$ values exhibit a pronounced concentration dependence. The **TMC-2** $\mu\beta$ rapidly increases as the concentration falls in the range of 10^{-3}–10^{-5} M, with $\mu\beta$ saturating at a large value of $-24\,000 \pm 4320 \times 10^{-48}$ esu at 5×10^{-6} M (Figure 8A). Significant deaggregation of **TMC-3** in CH$_2$Cl$_2$ occurs at lower concentrations, in the range 10^{-5}–10^{-6} M (Figure 8B), with an unprecedented $\mu\beta$ value of $-488\,000 \pm 48\,800 \times 10^{-48}$ esu measured at 8×10^{-7} M. The **TM-2** $\mu\beta$ exhibits similar concentration dependence in CH$_2$Cl$_2$, with a $\mu\beta$ value of $-315\,000 \pm 56\,700 \times 10^{-48}$ esu measured at 1×10^{-6} M (Table S3). From the computed μ values[44] we estimate $\beta_{0.65eV} \approx 8450, 890,$ and 9800×10^{-30} esu for **TM-2**, **TMC-2**, and **TMC-3**, respectively.

TMC $\mu\beta$ values measured in highly polar DMF are considerably less sensitive to concentration. The $\mu\beta$ of **TMC-2** (Figure 8A) begins to saturate at ∼5×10^{-5} M, with $\mu\beta = -5620 \pm 618 \times 10^{-48}$ esu at 5×10^{-6} M, while the $\mu\beta$ values of **TMC-3** (Figure 8B) still exhibit a gentle increase up to the highest dilution, with $\mu\beta = -84\,000 \pm 10\,080 \times 10^{-48}$ esu measured at 1.1×10^{-6} M. Similarly, the **TM-2** $\mu\beta$ in DMF exhibits saturation in dilution, with $\mu\beta = -49\,000 \pm 9800 \times 10^{-48}$ esu measured at 1×10^{-5} M.
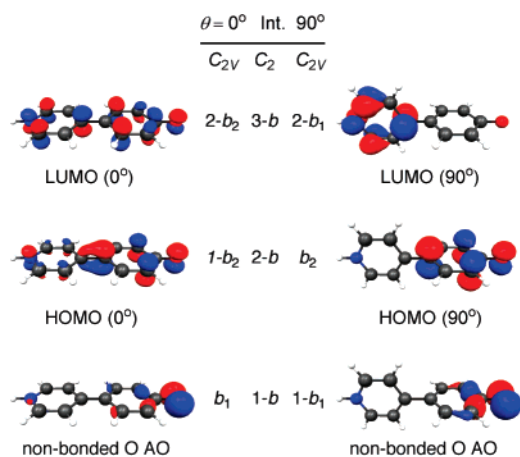
Electro-Optic Measurements on TMC-Based Poled Guest–Host Polymers. Poly(vinylphenol) films containing 10 wt % **TMC-2** and 5 wt % **TMC-3**, poled at 100 V/μm, give nonresonant r_{33} values of 48 and 330 pm/V, respectively, as
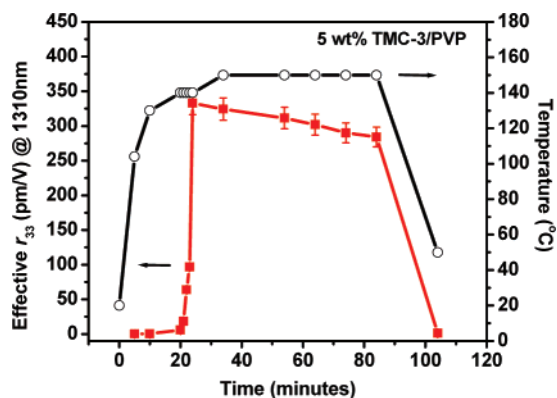
Figure 9. In situ poling and Teng−Man direct EO measurements on a polyvinylphenol (PVP) film containing 5 wt % **TMC-3**, poled at 100 V/μm.

Figure 10. Active space orbitals of model chromophore **TM-1′**. The symmetry labels are shown for the C_{2v} extrema ($\theta = 0°$ and 90°) as well as for the intermediate (C_2 symmetry) twist angles.

determined by Teng−Man electro-optic measurements at 1310 nm. Figure 9 shows a typical profile for in situ poling and Teng−Man measurement on 5 wt % **TMC-3**/PVP guest−host films. Under the applied DC electric poling field, the effective r_{33} undergoes a rapid increase when the temperature rises to ∼140 °C (the DSC-derived T_g of 5 wt % **TMC-3**/PVP is ∼148 °C) and reaches a saturation value of 330 pm/V when temperature is held at 140 °C. Further temperature increases result in a slow decrease of r_{33}, and when heating is removed, the r_{33} quickly drops to the noise level. This poling behavior presumably reflects the strong aggregation tendency of these zwitterions, which is also observed in less polar matrices, e.g., amorphous polycarbonate (APC, $\epsilon_r = 3$ vs 4.5 for PVP), where only very low EO responses are observed.

Computational Results. Calculations aimed at determining the lowest energy states yield orbital and state correlation diagrams for **TM-1′** as a function of torsional coordinate (Figure 10). The states chosen here are the lowest three states, two of which certainly correspond to the well-known inter-ring charge transfer in the twisted chromophores. In addition to identifying the lowest two states (Ψ_D and Ψ_Z), the second excited state was also investigated to determine whether higher energy states could contribute strongly to the observed nonlinear response properties. During the investigation of the vertical excitation spectrum of **TM-1′** it was found that when the CAS active space is expanded from the SS-CASSCF(2,2) to a SA3-CASSCF(4,3) active space, hence including the in-plane oxygen p AO and its

electrons, a second excited state appears fairly close in energy to the first excited state over a wide range of twist angles. The molecular orbitals which comprise the active space are shown in Figure 10. The SA3-CASSCF(4,3) potential-energy surfaces of the three lowest states of **TM-1′** are shown in Figure 11. It can be seen how these states change upon application of a dipolar field, which is intended to simulate the effects of a polar solvent medium. At a twist angle of 90°, the nonlinear response (β) was computed as the finite-second derivative of the dipole moment with respect to an additional applied field.

Discussion

Tictoid Chromophore Synthetic Strategies and Stability Characteristics. The formation of highly encumbered substitution patterns via the coupling of two arenes possessing bulky *ortho* substituents, specifically the synthesis of the tetra-*ortho*-methylbiaryl cores of the **TM** and **TMC** chromophore skeletons, presents a nontrivial synthetic challenge. We chose Suzuki methodology since it has previously demonstrated excellent tolerance to steric constraints among the catalytic cross-coupling reactions useful for unsymmetrical biaryl synthesis.[18,55] Employing a highly active Pd(0)/**DCPPP** Suzuki catalyst,[18] 4-bromo-pyridine *N*-oxide **1** can be coupled with boronic acid **2** to afford the key tetra-*ortho*-methylphenylpyridine core **3** in 53% yield (Scheme 1). Use of the pyridine *N*-oxide precursor here is crucial since the corresponding pyridine species evidence a pronounced sluggishness in the present coupling process for reasons possibly involving coordinative inhibition at the Pd center.[16] Interestingly, the *N*-oxide functionality does not appear to induce detrimental oxidation of the Pd(0) form of the catalyst here.

Another synthetic challenge involved in the **TMC** syntheses is the synthesis of twisted biaryl iodide **11**. This is crucial not only for facilitating the Heck coupling process in the **TM-2** synthesis, but also for enabling dicyanomethanide group introduction into the **TMC** skeletons, a transformation which cannot be efficiently achieved via nucleophilic triflate substitution[56] at **8**. Converting phenol **6** into aryl halides, which can subsequently undergo cross-coupling with active methylene regents such as malononitrile in the presence of Pd catalysts,[57] is thereby crucial to the **TMC** synthetic strategy. The only examples in the literature for the effective direct conversion of phenols to aryl halides, such as the thermolysis of a phenol-triphenylphosphine dibromide adduct[58] and displacement of triflate by iodide or bromide,[59] were unsuccessful in the present case. We therefore devised an effective new strategy for converting phenol **6** to iodide **11** by combining Pd-catalyzed aryl triflate amination[60] with arylamine-to-aryl halide conversion[61] (Scheme 1). The

(55) (a) Suzuki, A. *Proc. Jpn. Acad. Ser. B* **2004**, *80*, 359. (b) Bellina, F.; Carpita, A.; Rossi, R. *Synthesis* **2004**, *15*, 2419. (c) Kotha, S.; Lahiri, K.; Kashinath, D. *Tetrahedron* **2002**, *58*, 9633. (d) Johnson, M. G.; Foglesong, R. J. *Tetrahedron Lett.* **1997**, *38*, 7001. (e) Miyaura, N.; Suzuki, A. *Chem. Rev.* **1995**, *95*, 2457.
(56) (a) Atkinson, J. G.; Wasson, B. K.; Fuentes, J. J.; Girard, Y.; Rooney, C. S.; Engelhardt, E. L. *Tetrahedron Lett.* **1979**, *20*, 2857. (b) Williams, H. W. R.; Rooney, C. S.; Bicking, J. B.; Robb, C. M.; De Solms, S. J.; Woltersdorf, O. W.; Cragoe, E. J. *J. Org. Chem.* **1979**, *44*, 4060.
(57) (a) Uno, M.; Seto, K.; Takahashi, S. *J. Chem. Soc., Chem. Commun.* **1984**, 932. (b) Gao, C.; Tao, X.; Qian, Y.; Huang, J. *Chem. Commun.* **2003**, 1444.
(58) Wiley, G. A.; Hershkowitz, R. L.; Rein, B. M.; Chung, B. C. *J. Am. Chem. Soc.* **1964**, *86*, 964.
(59) Prugh, J. D.; Alberts, A. W.; Deana, A. A.; Gilfillian, J. L.; Huff, J. W.; Smith, R. L.; Wiggins, J. M. *J. Med. Chem.* **1990**, *33*, 758.
(60) (a) Wolfe, J. P.; Buchwald, S. L. *J. Org. Chem.* **1997**, *62*, 1264. (b) Louie, J.; Driver, M. S.; Hamann, B. C.; Hartwig, J. F. **1997**, *62*, 1268.
(61) Kosynkin, D.; Bockman, T. M.; Kochi, J. K. *J. Am. Chem. Soc.* **1997**, *119*, 4846.
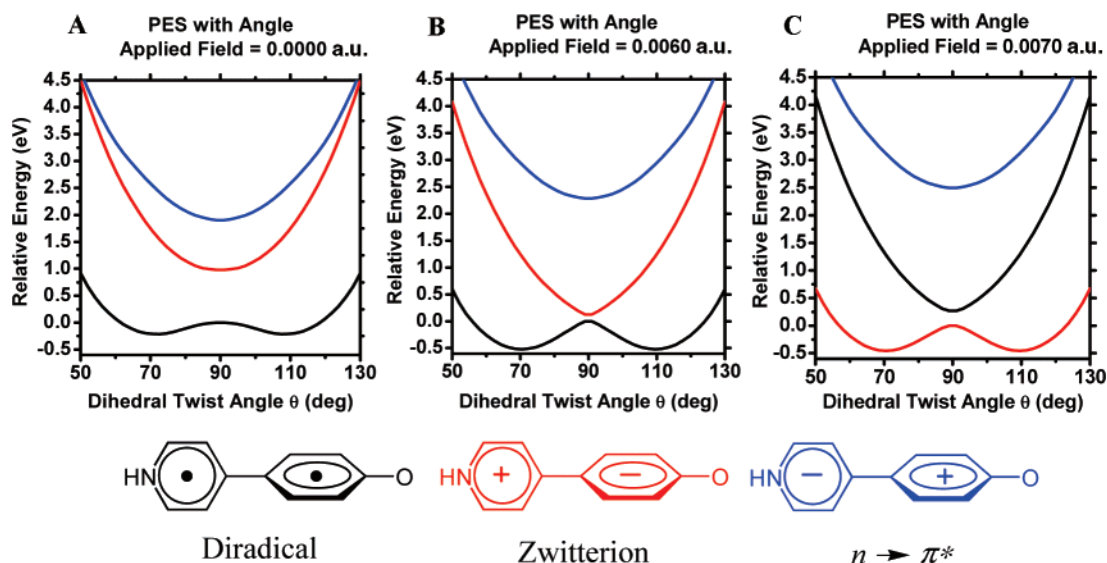
Figure 11. Potential-energy surfaces (PESs) for the lowest three singlet states of **TM-1'** as a function of angle and applied field (A–C). The field is applied in the longitudinal direction. The black curve corresponds to a state which has a diradical wave function at $\theta = 90°$, the red curve corresponds to a state which is a zwitterion at $\theta = 90°$, and the blue curve represents the PES for the state formed from an $n \rightarrow \pi^*$ transition.
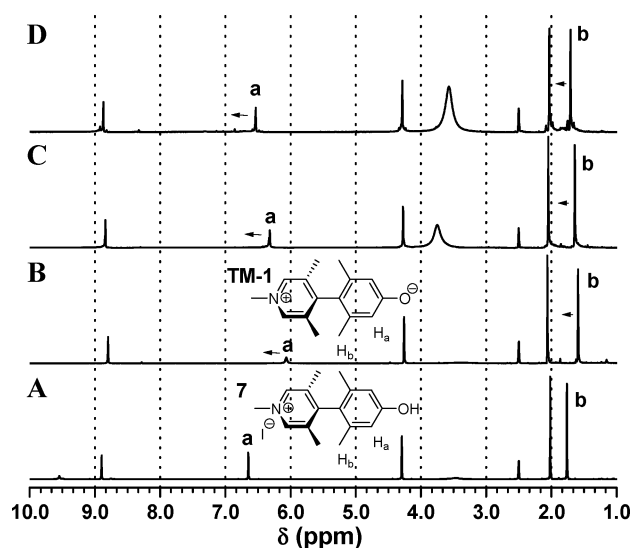
Figure 12. ^{1}H NMR spectra (400 MHz, 25 °C) of precursor **7** (A), **TM-1** (B) in dry DMSO-d_6, and **TM-1** in DMSO-d_6 solution exposed in air during the period of 1 (C) and 5 (D) days.

overall yield of this four-step phenol-to-aryl iodide conversion is 65% and therefore represents an efficient general route for phenol-to-aryl halide conversion.

The product **TM** and **TMC** chromophores exhibit very different chemical and thermal stability characteristics. **TM** chromophores exhibit considerable sensitivity to moisture. Dark red **TM-1** solid quickly bleaches when exposed to moisture, implying that protonation may take place at the aryl O⁻ group, evidenced by ^{1}H NMR spectroscopy in DMSO-d_6 (Figure 12). The signals from phenylene ring and methyl protons adjacent to the aryl O⁻ group (H_a and H_b, Figure 12) are displaced significantly downfield when the NMR solution is exposed to moisture. This marked proton affinity is consistent with a twist-induced reduction in inter-ring π conjugation, thereby resulting in a dominant charge-separated zwitterionic ground state, describable as a noncommunicating phenoxide anion adjacent to a pyridinium cation. Here the phenoxide portion is expected to be a strong Lewis base (the pK_a of the related 3,5-

dimethylphenol is 10.2).[62] Such a charge-localized structure may also account for the low thermal stability observed in **TM-1**, where the pyridinium *N*-methyl substituent undergoes alkylative migration to the aryl O⁻ group to form neutral 4-(4-methoxy-2,6-dimethyl-phenyl)-3,5-dimethyl-pyridine (**4**, Scheme 1) when heated to 200 °C in vacuum, reflecting the strong nucleophilicity of the aryl O⁻ group. **TM-2** exhibits slightly enhanced stability compared with **TM-1**, probably due to the steric protection of the two bulky *ortho tert*-butyl substituents adjacent to the aryl O⁻ group. In addition to moisture sensitivity, both **TM** chromophores have only modest solubilities in most organic solvents, even in the case of *N*-octyl-functionalized **TM-2**.

In marked contrast to the **TM** chromophores, the **TMC** chromophores are air and moisture stable and readily purifiable by conventional column chromatography. Thermogravimetric analysis indicates that these materials have very high thermal stability ($T_d \approx 306$ °C for **TMC-2** and 330 °C for **TMC-3**, Figure S2), while ^{1}H NMR spectroscopy indicates stability in DMSO-d_6 solution at 150 °C for periods of hours under air. This marked chemical and thermal robustness doubtless results from introduction of the charge-stabilizing dicyanomethanide functionality, where negative charge is delocalized by two strong electron-withdrawing cyano groups through resonant delocalization (also observable in the crystallographic data, vide supra). Here the dicyanomethanide portion is expected to be a weak Lewis base (the pK_a of related phenylmalononitrile is 4.2).[63] For donor–acceptor EO chromophores, the **TMC** series is a noteworthy example of introducing a stabilized anion into a twisted π-electron system zwitterion, where significant charge stabilization through a quinoidal limiting resonance structure is unlikely.

Tictoid Chromophore Structural Characteristics. The combination of single-crystal XRD data with optical, IR, and NMR spectroscopies, both in the solid state and in solution, provides fundamental architectural and electronic structural

(62) *Handbook of Organic Chemistry*; Dean, J., Ed.; McGraw-Hill: New York, 1987.
(63) Algrim, D.; Bares, J. E.; Branca, J. C.; Bordwell, F. G. *J. Org. Chem.* **1978**, *43*, 5024.

insight into these new tictoid chromophores. The most important feature revealed from the crystallographic analyses of the target chromophores as well as of their synthetic precursors is the consistently large and relatively uniform arene−arene dihedral twist angle (80−89°; Table 1), suggesting that the tetra-*ortho*-methylbiaryl substitution pattern indeed provides sufficient steric encumbrance to achieve the desired inter-ring staggering, an anticipated[15] prerequisite for large molecular hyperpolarizabilities in such twisted π-electron system chromophores. Furthermore, it can be seen that the magnitude of this twist is governed primarily by sterics and essentially independent of chromophore architecture and charge distribution. Indeed, neutral, positively charged, and zwitterionic molecules all exhibit comparable twist angles (Table 1). A number of earlier studies have shown that the electronic structure of merocyanines can be described as some hybrid of the quinoid and benzenoid limiting structures and that any external perturbation, such as solvation or an external electric field, can lead to stabilization of the charge-separated benzenoid structure.[4d] The electronic structures of these chromophores are therefore highly dependent on the state of the materials and medium surrounding the molecules.


benzenoid   **quinoid**
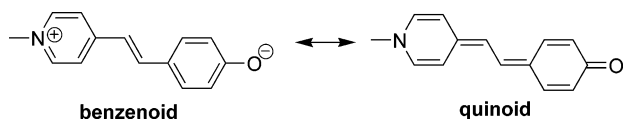
In the present tictoid chromophores, the steric encumbrance-induced twist leads to a pronounced enforced reduction in inter-ring π conjugation, and this in turn leads to aromatic stabilization of the resultant pyridinium and phenoxide/phenyldicynomethanide fragments, resulting in a chemically, thermally robust, dominant charge-separated zwitterionic ground state. Molecular electronic structure should be predominantly governed by the twist and affected by external perturbations such as dielectric constant. This solid-state zwitterionic structural assignment is supported by a full complement of single-crystal metrical parameters, such as the (ring)C−C(ring), (ring)C−O, and (dicyanomethanide)C−C(aryl) distances, and the bond length patterns within the pyridinium and phenoxide/phenyldicynomethanide fragments.

Importantly, NOE NMR measurements of the **TMC** twist angle in solution confirm that solid-state twist angle persists in solution. Optical spectroscopies provide further evidence for a zwitterionic tictoid ground state in the solution phase. The tictoid spectra exhibit both inter-ring HOMO−LUMO charge-transfer (CT) excitations as well as intra-subfragment transitions within the pyridinium and phenyl (stilbenyl in **TM-2** and **TMC-3**) fragments. This implies that the tictoid ground state is better described in terms of linked pyridinium acceptor and phenoxide/phenyldicynomethanide donor portions. The relatively small oscillator strengths in the CT band appear to reflect the pronounced reduction in inter-ring π conjugation and are consistent with large inter-ring dihedral angles observed in the X-ray diffraction studies. Furthermore, the strong *negative* solvatochromism effects observed in the **TMC** optical spectra indicate that the ground-state dipole moment is substantially larger than in the excited state, consistent with a dominant zwitterionic ground-state description.

The twist chromophore IR vibrational spectroscopic features provide structural information consistent with that obtained from the XRD analyses and optical spectroscopic studies. The typical

vibrational spectroscopic benzenoid phenoxide ring stretching features and the strong reduction of the quinoid C=O stretching frequency in the **TM** chromophores and the almost pure phenyldicynomethnide anion-like C≡N stretching frequency in the **TMC** chromophores clearly support a dominant zwitterionic structure in the ground state. Comparative solid-state ¹³C NMR, optical, and IR spectroscopic studies provide additional structure−property information regarding solution phase vs solid phase **TM** and **TMC** properties. Close correspondence between solid-state ¹³C NMR, optical, and IR spectra and those recorded in solution suggest that the large inter-ring dihedral twist angle and zwitterionic ground state observed in the solid state persist essentially unchanged in the solution phase and that it is reasonable to interpret **TMC** solution-phase properties (such as linear/nonlinear optical response) in terms of solid-state crystal structure metrical parameters (in particular the twist angle).
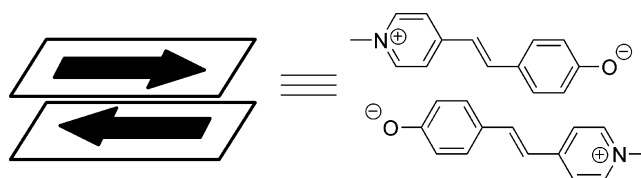
Aggregation Properties. The aggregation of dipolar NLO chromophores has been identified as an important issue in understanding basic molecular EO response as well as in applications.[43,64] In the case of merocyanine dyes, the centrosymmetric nature of the dye aggregation is clearly anticipated by the nature of possible electrostatic dipole−dipole interactions and was recently verified experimentally.[43]

This type of aggregation is obviously detrimental to applications in electro-optics where a microstructurally polar chromophore arrangement is essential. It is only by removing the impediment of aggregation that the exceptional molecular hyperpolarizability properties in the present tictoid chromophores can be accessed and fully exploited. Thus, a full investigation and understanding of the nature of tictoid chromophore aggregation is important. As might be expected, the new tictoid chromophores described here exhibit significant aggregation tendencies in the solid state and concentrated solutions, evidenced from X-ray diffraction data and concentration-dependent optical absorption, fluorescence, and PGSE NMR spectroscopic studies. These results are entirely reasonable considering the large computed dipole moments.[44]

Analysis of the tictoid zwitterion packing in the crystalline state clearly shows the formation of centrosymmetric antiparallel dimers. Although the substituent-modulated intermolecular distances between tictoid molecules in the dimeric units are significantly larger than those observed in planar merocyanine zwitterion dimers (∼ 3.50 Å),[43] the very strong dipole moments in the highly charge-separated tictoid molecules still result in comparable or even larger electrostatic interactions (this can be readily seen from estimated binding energies compared with those of planar zwitterions, vide infra). These intermolecular distances depend principally on steric details. It can be seen in

(64) (a) Cross, G. H.; Hackman, N.-A.; Thomas, P. R.; Szablewski, M.; Palsson, L.-O.; Bloor, D. *Opt. Mater.* **2002**, *21*, 29. (b) Wüthner, F.; Yao, S. *Angew. Chem., Int. Ed.* **2000**, *39*, 1978. (c) Dalton, L. R.; Harper, A. W.; Robinson, B. H. *Proc. Natl. Acad. Sci. U.S.A.* **1997**, *94*, 4842.

Figure 1 that the **TMC-2** dimeric units have larger intermolecular distances separating monomers than in **TMC-1** dimeric units, clearly the result of accommodating the bulky *N*-alkyl chain. The relatively looser packing in **TMC-2** vs **TMC-1** can also be seen in the experimental crystal densities (1.110 g/cm^3 for **TMC-2** vs 1.184 g/cm^3 for **TMC-1**), which is also consistent with the reduced dimerization energy of **TMC-2** in solution compared with **TMC-1** (vide supra).

The strong aggregation tendency of **TMC-2** is further supported by concentration-dependent optical absorption spectra, exhibiting a pronounced blue shift and decrease of the CT excitation intensity upon increasing the concentration. Moreover, an isosbestic point is observed, supporting well-defined aggregation equilibria and indicating the formation of H-type antiparallel centrosymmetric aggregates,[43] in agreement with the X-ray diffraction data. The binding energetics, estimated by analyzing the **TMC-2** extinction coefficient as a function of concentration assuming a simplistic (but tractable) dimerization model, not unexpectedly indicate that the aggregation is weaker in more polar solvents, with derived binding constant $K_d = 250 \pm 30$ M^{-1} and Gibbs free energy $\Delta G°_d = -13.6 \pm 0.3$ kJ mol^{-1} in CH$_2$Cl$_2$ ($\epsilon_r^{25} = 8.93$) vs $K_d = 13300 \pm 1420$ M^{-1} and $\Delta G°_d = -23.5 \pm 0.3$ kJ mol^{-1} in less polar CHCl$_3$ ($\epsilon_r^{25} = 4.81$). The aggregation free energy is expected to be highly dependent on solvent polarity when the electrostatic interactions between two interacting monomer dipole moments dominate the binding forces.[47] These K_d and $\Delta G°_d$ values indicate stronger aggregation in **TMC-2** than in typical planar merocyanine zwitterions in the same solvents (e.g., the dye **HPOP** has a binding constant K_d of 520 M^{-1} and Gibbs free energy $\Delta G°_d$ of -15.2 kJ mol^{-1} in CHCl$_3$),[43] doubtless caused by the larger **TMC** molecular dipole moments,[44] clearly a consequence of the highly charge-separated ground states. Variable-concentration **TMC-2** and **TMC-3** fluorescence spectra in CH$_2$Cl$_2$ provide further evidence of **TMC** aggregation. The unexpected blue shift of the **TMC-2** fluorescence spectra for the H-type aggregates could conceivably be due to unusually slow radiationless relaxation between exciton-split states, resulting in **TMC-2** fluorescence from the higher energy state.[65] An alternative explanation for the inverse trend observed in the **TMC-2** fluorescence spectra invokes strong reabsorption.[66] In contrast, the **TMC-3** dimers exhibit more conventional red-shifted florescence. It can be seen that significantly higher concentrations are necessary to observe aggregation effects in **TMC-2** than for **TMC-3** in the same solvent, clearly a result of a much greater dipole moment in **TMC-3** than in **TMC-2**.[44]

HPOP
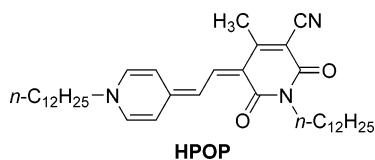
PGSE NMR spectroscopy provides additional, quantitative information on the state of **TMC** aggregation. Both **TMC-2** and **TMC-3** exhibit pronounced aggregation tendencies in CD$_2$-Cl$_2$ ($\epsilon_r^{25} = 8.93$), with **TMC-3** exhibiting substantially greater

(65) Park, J.-M.; Zhang, W.; Nakatsuji, Y.; Majima, T.; Ikeda, I. *Chem. Lett.* **2000**, *29*, 182.
(66) *Principles of Instrumental Analysis Chemistry,* 7th ed.; Skoog, D. A., Leary, J. L., Eds.; Saunders College Publishing: Philadelphia, 1996.

aggregation levels than **TMC-2**. At the highest accessible concentrations, **TMC-2** and **TMC-3** exhibit aggregation numbers of $N = 2.7$ and 2.5, respectively, implying that more complex aggregates than dimers are also present, consistent with the tetramer-like aggregates observed in **TMC** crystal structure data (Figure 1C). The aggregation numbers decrease upon dilution, tending toward $N = 1.0$ and revealing dissociation of aggregates in dilute solutions in the $10^{-3}-10^{-4}$ M concentration range for **TMC-2**, in good agreement with the optical spectroscopic data (Figure 7A, inset). **TMC-3** exhibits greater aggregation tendencies and is not exclusively monomeric even at 5×10^{-6} M, consistent with the results of the variable-concentration **TMC-3** fluorescence spectroscopy (Figure 7B). The aggregation numbers for both **TMC-2** and **TMC-3** in more polar DMSO-d_6 ($\epsilon_r^{25} = 46.45$) are close to 1.0 and almost independent of the concentration, clearly the result of the aforementioned strong polar solvation effects on aggregation.

Nonlinear Optical and Electro-Optic Properties. EFISH-derived $\mu\beta$ values for chromophores **TMC-2** and **TMC-3** in CH$_2$Cl$_2$ and DMF exhibit negative signs, indicating that the ground state is more polar than the excited state,[4d,10] in agreement with the observed negative solvatochromism (vide supra). In less polar CH$_2$Cl$_2$ (Figure 8), the $\mu\beta$ values exhibit a pronounced concentration dependence due to the aforementioned aggregation effects of a type previously reported for zwitterionic TCNQ derivatives.[64a] The comparison between EFISH and PGSE data over a wide range of concentrations shows good agreement with the trends in aggregation (Figure 8). The **TMC-2** $\mu\beta$ in CH$_2$Cl$_2$ rapidly increases as concentration falls, implying dissociation of (presumably centrosymmetric) aggregates. Indeed, the $\mu\beta$ approaches a maximum at concentrations where the PGSE measurements indicate the presence of greater than 80% monomer (Figure 8A). Again, **TMC-3** deaggregation trends in the EFISH data (Figure 8B) closely parallel those for the PGSE data, with $\mu\beta$ rapidly increasing at concentration levels where the monomer content is ~80% (Figure 8B) and saturating at an unprecedented $\mu\beta$ value of $-488\,000 \pm 48\,800 \times 10^{-48}$ esu at 1907 nm. The chromophore figure of merit, defined by $\mu\beta/M_w$, is as large as 945×10^{-48} esu, almost 20 times larger than the highest value of 46×10^{-48} esu previously reported.[3d] The off-resonance $\beta_{0.65eV}$ estimated from the computed μ values[44] is as large as 9800×10^{-30} esu. In recent elegant work,[11] Kuzyk estimated the fundamental limits of hyperpolarizability using quantum sum rules and found that the apparent limit for all the experimentally achieved hyperpolarizabilities in organic molecules falls far short of the fundamental limit by a factor of $10^{-3/2}$. For example, a chromophore having 22 π electrons and an absorption maximum of 540 nm, as in tictoid chromophore **TMC-3**, could possess a maximum nonresonant β as large as $20\,000 \times 10^{-30}$ esu according to Kuzyk's estimates. However, all βs achieved previously fall below an apparent limit of ~600×10^{-30} esu. For the first time, the βs achieved in the present tictoid chromophores approach the fundamental limit, clearly suggesting a new paradigm for organic electro-optics. The present results may provide insights into the reasons for this universal gap between the experimental β results and the fundamental limits.

The $\mu\beta$ values measured in highly polar DMF ($\epsilon_r^{25} = 37.8$) exhibit a less abrupt increase as concentration falls, a sign of a weaker aggregation in more polar DMF than in CH$_2$Cl$_2$ ($\epsilon_r^{25} =$

8.93), consistent with the PGSE data. That the magnitude of the EFISH-derived $\mu\beta$ is lower in more polar solvents has also been reported for other zwitterionic chromophores and theoretically investigated[4d,67] and is in agreement with the present theoretical study. It was found previously that the first hyperpolarizabilities of typical zwitterionic molecules exhibit remarkable solvation effects.[4d] β values are small and positive in the gas phase but become negative with increasing solvent polarity. They remain negative in all polar solvents and reach a maximum at a moderate $\epsilon_r \approx 6-8$ and then again decrease slowly with further increase of ϵ_r. This behavior is ascribed principally to the change in charge distribution and dipole moment. Once the structure is dominated by the zwitterionic limit, β values decrease with increasing solvent polarity.[4d,67]

The SA3-CASSCF(4,3) computations in this work provide a new rationale for these exceptional hyperpolarizabilities and the observed solvation effects on hyperpolarizabilities. It was recently found[68] that SS-CASSCF(2,2) gas-phase calculations afford a zwitterionic ground state (Ψ_Z) for the fully methylated chromophore **TM-1** at a 90° twist angle. In agreement with this result, in this work it is also found that SS-CASSCF(4,3) and SA2-CASSCF(2,2) calculations lead to this seemingly unphysical result. Increasing the active space and adding the second excited state (SA3-CASSCF(4,3)) affords a dominant diradical ground state (Ψ_D) in the gas phase in agreement with the much larger SS-CASSCF(14,13) calculations.[68] The first excited state is easily characterized as being the zwitterionic state (Ψ_Z), and the second excited state corresponds to the product ($\Psi_{n\rightarrow\pi^*}$) of a $n \rightarrow \pi^*$ transition. Figure 11 reveals that the potential-energy surfaces of the lowest three states are very dependent upon the strength of an external applied dipolar field (to simulate polar solvation). In the gas phase ($F = 0.0$ au) at $\theta = 90°$, the CI coefficients suggest that the diradical state is the ground state. However, applying a dipolar field strength of $F = 0.007$ au to simulate polar solvation leads to an exclusive zwitterionic ground state. At an intermediate field strength of $F = 0.006$ au, the energy differences between the two states at $\theta = 90°$ is negligible. As suggested by the sum-over-states (SOS) equation, this small energy difference should lead to a very large static β. At 90° twist angles, the SA3-CASSCF-computed static hyperpolarizabilities (β) in the gas phase at field strengths of 0.006 and 0.007 au are 1.1×10^1, 5.7×10^4, and 1.7×10^4 (10^{-30} esu), respectively, in agreement with a previous SA-CASSCF investigation[68] where the computed β was found to be very small in the gas phase. At higher field strengths, the β values in the present study are found to be 3 orders of magnitude larger than those in the gas phase and negative, in accord with experiment. Further increasing the dipolar field strength from 0.006 to 0.007 au yields a significant decrease in hyperpolarizability, consistent with the remarkable solvation effects observed for the experimental hyperpolarizabilities.

With knowledge of the **TMC** potential energy surfaces, a number of predictions can be made about the nonlinear response (β) by employing the sum-over-states (SOS) formula. At $\theta = 90°$, the diradical state wave function term symbol is $^1A_2$,

whereas the zwitterion and $n \rightarrow \pi^*$ state term symbols are both $^1A_1$. When the ground-state wave function is a diradical (in the gas phase), and the first two excited states, which would be expected to contribute most strongly to the ground state for energetic reasons, are dipole-disallowed transitions; hence, β should be very small. When a dipolar field is applied, the zwitterionic state shifts to become the ground state. Since it has an allowed dipole transition with the $n \rightarrow \pi^*$ state, this state interaction is expected to contribute significantly to the β of the ground-state zwitterion. Further increasing the electric field begins to lower the energy of the zwitterionic state relative to the excited-state manifold; hence, β begins to decrease with increasing field (also observed here experimentally).

In evaluating the present EFISH results, external electric field effects on reducing the chromophore aggregation must also be taken into account, as shown in previous studies.[43,69] This effect may be expected to be significant if the species in aggregation equilibrium strongly differ in dipole moments, as observed for the monomeric and dimeric species in the present zwitterionic chromophores. The competition between internal dipolar interactions leading to aggregation and the external electric fields leading to dissociation could conceivably shift the aggregation equilibrium to some degree. Taking a simple dimerization model, the new dimerization constant under an applied electric field, K_d^E, is given by eq 14[43]

$$K_d^E = K_d \exp(-\Delta G_d^E/RT) \tag{14}$$

where ΔG_d^E is the electric field-induced contribution to the Gibbs free energy of the dimerization, which can be estimated, assuming a vanishing dimer dipole moment, by eq 15[43]

$$\Delta G_d^E = \frac{N_A L^2 \mu_g^2 E^2}{3kT} \tag{15}$$

where N_A is Avogadro's number, L a Lorentz local field factor given by $L = (\epsilon_r + 2)/3$,[70] μ_g the dipole moment of the chromophore, and E the electric field. For chromophore **TMC-2** in CH_2Cl_2 with a DFT-derived ground-state dipole moment of 27.0 D, a Lorentz local field factor of $L = 3.64$, and an estimated dimerization constant $K_d = 246$ M^{-1} and applying an EFISH field of 7×10^6 V/m, the field-dependent dimerization constant K_d^E is then estimated to be 222 vs 246 M^{-1} in the absence of the field. As can be seen, the present electric fields in the EFISH measurement are insufficient to greatly affect the aggregation equilibria.

Teng−Man[31] experiments on poled **TMC-2**- and **TMC-3**-based guest−host polyvinylphenol (PVP, $\epsilon_r = 4.5$) films reveal very large EO coefficients (r_{33}) at 1310 nm, confirming the exceptional hyperpolarizabilities in these chromophores. The exact poling behavior of **TMC-3**/PVP guest−host films (Figure 9) presumably reflects the strong aggregation tendencies of these zwitterions as discussed above, which is also observed in less polar matrices, e.g., amorphous polycarbonate (APC, $\epsilon_r = 3$), where only very weak EO responses are observed. Chromophore dipolar aggregation is clearly detrimental to the performance of EO materials. The aforementioned aggregation studies on **TMC** chromophores demonstrate how the aggregation can be characterized quantitatively in solution and how molecular modification of the chromophores can be utilized to minimize aggregation. While the dimerization constant determined in

(67) Ray, P. C. *Chem. Phys. Lett.* **2004**, *395*, 269.
(68) Isborn, C. M.; Davidson, E. R.; Robinson, B. H. *J. Phys. Chem. A* **2006**, *22*, 110.
(69) (a) Wortmann, R.; Rösch, U.; Redi-Abshiro, M.; Würthner, F. *Angew. Chem., Int. Ed.* **2003**, *42*, 2080. (b) Liptay, W.; Rehm, T.; Wehning, D.; Schanne, L.; Baumann, W.; Lang, W. *Z. Naturforsch. A* **1982**, *37*, 1427.
(70) Wortmann, R.; Bishop, D. M. *J. Chem. Phys.* **1998**, *108*, 1001.

solution may not directly correlate with the degree of the aggregation in host polymers, it is reasonable to use it to estimate the order of magnitude of the aggregation effects in these guest–host materials. For example, the polarity of PVP ($\epsilon_r = 4.5$) is close to that of chloroform ($\epsilon_r = 4.8$), and the **TMC-2** dimerization constant K_d is estimated to be 13 300 M^{-1} in chloroform (vide supra). We can then estimate that for **TMC-2** $K_d \approx 13\ 300\ M^{-1}$ in PVP. A **TMC-2** doping level of 10 wt % in PVP corresponds to a concentration of $c_0 \approx 0.28$ M, and it follows from K_d that monomer concentration $c_M \approx 0.003$ M, so that about 99% of the **TMC-2** chromophore molecules are predicted to be present in the form of dimers in PVP at room temperature. However, upon applying poling field (100 V/μm in the present experiments), we can then derive the field-dependent dimerization constant $K_d^E = 7.14\ M^{-1}$ at room temperature according to eqs 14 and 15 (with a Lorentz local field factor of $L = 2.17$). This is a significant shift of the dimerization equilibrium with the monomer concentration c_M changing to 0.11 M, so that ~40% of the **TMC-2** chromophores is present as the dissociated monomer in the host at room temperature. Furthermore, since the present dimerization of the chromophore is an exothermic reaction with an expected negative dimerization enthalpy and entropy,[43] an increase of the temperature will result in the decrease of dimerization constant K_d. Therefore, upon heating the polymer matrix during the poling, a greater proportion of the chromophore will be present as dissociated monomers. It can be seen that there is still considerable room to realize the optimal values offered by such exceptional hyperpolarizabilities. Judging from the aforementioned crystallographic observations and spectroscopic aggregation studies, it is clear that bulky skeletal substituents should prevent close aggregation, and from recent successes that steric inhibition has had in dramatically improving bulk EO response,[71] there is reason to believe that the present aggregation issues can be similarly addressed and that further enhanced r_{33} values will be achieved.

Conclusions

A series of theory-inspired, unconventional twisted π-electron system EO chromophores (**TM** and **TMC**) have been designed and synthesized. Efficient synthetic approaches were developed to realize these sterically hindered zwitterionic biaryls. All of these new compounds have been fully characterized via conventional analytical/spectroscopic techniques. The **TMC** chromophores exhibit excellent thermal and chemical stability. Crystallographic analysis of these molecules reveals large and nearly invariant ring–ring dihedral twist angles (80–89°) and highly charge-separated zwitterionic ground states. This twist is governed primarily by the *o,o',o'',o'''*-substituted biaryl core

and practically independent of chromophore architecture/charge distribution. NOE NMR measurements confirm that solid-state twist angle persists in solution. Optical spectroscopy of these chromophores reveals a twist-induced reduction of inter-ring charge transfer (CT) and strong negative solvatochromism, evidence of charge-separated zwitterionic structure in solution. The solid-state vs solution-phase ^{13}C NMR, IR, and optical spectroscopic studies on these chromophores further support that zwitterionic ground-state structural characteristics observed in solid-state persist virtually unchanged in the solution phase and that these chromophores exhibit a strong tendency for centrosymmetric aggregation in concentrated solution. Detailed information on the state of this aggregation, such as aggregation model, level, and binding energies, has been provided by a combination of techniques, including concentration-dependent optical spectroscopy, pulsed field gradient spin–echo (PGSE) NMR measurements, and X-ray crystallography. Most importantly, exceptional molecular hyperpolarizabilities of these unconventional chromophores have been achieved in this work, with EFISH-derived nonresonant $\mu\beta$ values as high as $-488\ 000 \times 10^{-48}$ esu at 1907 nm. Preliminary direct Teng–Man reflection measurements on guest–host poled polymers containing these chromophores reveal a very large electro-optic coefficient (r_{33}) of ~ 330 pm/V at 1310 nm. Aggregation effects are also observed in these measurements and shown to be an issue to be addressed in future EO applications. SA-CASSCF computations provide a new rationale for these exceptional hyperpolarizabilities and demonstrate significant solvation effects on hyperpolarizabilities in good agreement with experimental results. In summary, this work shows twisted π-electron system chromophores to be promising candidates for EO applications and provides new insights into the design of molecule-based EO materials.

Supporting Information Available: Synthetic details and characterization, crystallographic data (CIF), NOE data, EFISH data, setup for in situ poling and Teng–Man EO measurements, TGA plot for **TMC-2** and **TMC-3**, PGSE NMR data, and CV plots of **TM** and **TMC** chromophores. This material is available free of charge via the Internet at http://pubs.acs.org.

JA0674690

(71) (a) Zhang, C.; Sun, S.-S.; Bonner, C. E.; Kim, S.; Fetterman, H. R.; Dalton, L. R. *SPIE Proc.* **2005**, *6020*, 56. (b) Luo, J.; Ma, H.; Haller, M.; Jen, A. K.-Y.; Barto, R. R. *Chem. Commun.* **2002**, 888. (c) Ma, H.; Chen, B. Q.; Sassa, T.; Dalton, L. R.; Jen, A. K. Y. *J. Am. Chem. Soc.* **2001**, *123*, 986. (d) Robinson, B. H.; Dalton, L. R. *J. Phys. Chem. A* **2000**, *104* (20), 4785. (e) Harper, A. W.; Sun, S.; Dalton, L. R.; Garner, S. M.; Chen, A.; Kalluri, S.; Steier, W. H.; Robinson, R. H. J. *Opt. Soc. Am. B* **1998**, *15*, 329.